

1 **Tropical cyclone genesis potential across palaeoclimates.**

2

3 **J. H. Koh and C. M. Brierley**

4 Department of Geography, University College London, London WC1E 6BT, UK

5 Correspondence to: C. M. Brierley (c.brierley@ucl.ac.uk)

6

7 **Abstract**

8 The favourability of the Pliocene, Last Glacial Maximum (LGM) and the mid-Holocene for
9 tropical cyclone formation is investigated in five climate models. This is measured by a
10 genesis potential index, derived from large-scale atmospheric properties known to be related
11 to storm formation. The mid-Pliocene and LGM characterise periods where carbon dioxide
12 levels were higher and lower than preindustrial respectively, while the mid-Holocene differed
13 primarily in its orbital configuration. The cumulative global genesis potential is found to be
14 fairly invariant across the palaeoclimates in the multi-model mean. Despite this all ensemble
15 members agree on coherent responses in the spatial patterns of genesis potential change.

16

17 During the Pliocene and LGM, changes in carbon dioxide led to sea surface temperature
18 changes throughout the tropics, yet the potential intensity (a measure associated with
19 maximum tropical cyclone strength) is calculated to be relatively insensitive to these changes.
20 Changes in tropical cyclone genesis potential during the mid-Holocene are found to be
21 asymmetric about the Equator: being reduced in the northern hemisphere, but enhanced in the
22 southern hemisphere. This is clearly driven by the altered seasonal insolation. Nonetheless,
23 the enhanced seasonality drove localised changes in genesis potential, by altering the strength
24 of monsoons and shifting of the Inter-tropical Convergence Zone. Trends in future tropical
25 cyclone genesis potential are neither consistent between the five models studied, nor with the
26 palaeoclimate results. It is not clear why this should be the case.

27 **1 Introduction**

28 Tropical cyclones (TC) constitute one of the most powerful forces of nature and can cause
29 severe destruction to human life and property. How TC genesis may change in the face of

1 climate change is thus an area of strong interest. Past studies using high resolution general
2 circulation models (GCMs) have generally suggested that cyclone intensity would strengthen,
3 yet cyclone genesis would decline in a warming climate (Knutson et al. 2010). However,
4 recent analyses of future simulations performed as part of the Coupled Model
5 Intercomparison Project Phase 5 (CMIP5) appear equivocal: statistical downscaling indicates
6 an increase in both cyclone intensity and genesis (Emanuel 2013); dynamical downscaling
7 indicates an increase in intensity combined with a reduction in frequency (Knutson et al.,
8 2013); tracking algorithms of global coupled models do likewise (Camargo, 2013); large-
9 scale cyclogenesis indices have shown both frequency increases (Emanuel, 2013) and
10 decreases (Camargo, 2013).

11

12 Understanding past climates provides a means for scientists to contextualise future climate
13 change impacts. Palaeoclimates with altered climate forcings, such as the elevated levels of
14 carbon dioxide during the Pliocene period, may provide clues on how the trend of cyclone
15 genesis would respond to ongoing anthropogenic emissions of greenhouse gases.

16

17 The mid-Piacenzian warm portion of the mid-Pliocene (around 3 million years ago,
18 henceforth “Pliocene”) was a recent episode in Earth’s geological history where mean global
19 temperatures were warmer by 2-3°C compared to modern times (Haywood et al. 2013), but
20 the warming was not constant across the globe. Sea surface temperature (SST) anomalies
21 were more pronounced at the higher latitudes (up to 20°C in the high Arctic; Ballantyne et al.
22 2009), while the lower latitudes exhibited minimal change in places (Dowsett et al., 2010).
23 The geography of the continents and oceans were relatively similar to earth’s current
24 configuration (Haywood et al. 2011). Carbon dioxide levels were at near present day during
25 the mid-Pliocene (Pagani et al. 2009). There is potential of using the Pliocene to learn about
26 the equilibrium state of earth’s warm climate following anthropogenic greenhouse gas
27 influence (Haywood et al. 2009).

28

29 The icy climate of the Last Glacial Maximum (LGM) at 21ka serves as a contrast to both the
30 warm climates of the Pliocene and the 20th Century. Proxy estimates by Annan and
31 Hargreaves (2013) suggest that LGM tropical SST was around 1.6°C lower than preindustrial,

1 while global surface air temperatures were 3.1-4.7°C cooler. Given the relatively similar
2 orbital parameters controlling earth's solar insolation during the Pliocene, LGM and
3 preindustrial periods, the focus of the Palaeoclimate Model Intercomparison Project (PMIP)
4 on these eras help facilitate studies that examine the effect of carbon dioxide concentration
5 changes on the tropical climate (Table 1).

6

7 On the other hand, simulations for the mid-Holocene epoch at 6ka differ from preindustrial
8 conditions mainly in the orbital parameters that result in an increased insolation in the high
9 latitudes. The tropical region of the mid-Holocene period might have encountered slightly
10 elevated sea-surface temperatures (SST) of around 1 °C (Gagan et al. 1998), although recent
11 studies indicate some uncertainty in terms of negative SST anomaly for regions such as the
12 western Indian Ocean (Kuhnert et al. 2014). Despite the limited proxy record agreement on
13 whether tropical oceans may have warmed (Koutavas et al. 2002; Rimbu et al. 2004; Stott et
14 al. 2004), prior PMIP simulations suggest SST in the northern hemisphere was generally
15 warmer by less than 1 °C in the mid-Holocene period compared to the preindustrial era, and
16 the southern hemisphere might have been slightly cooler (Braconnot et al. 2007).

17

18 Given the lack of data on tropical cyclone frequency for deep-time palaeoclimates, model
19 simulation studies cannot seek to verify model response on cyclone formation, but rather aim
20 to describe tropical cyclone trends with the assumption that signals would be detectable by
21 using indicators such as cyclogenesis potential. Using PMIP Phase 2 (PMIP2) data, studies
22 have been conducted to investigate indices related to TC genesis activity during the LGM and
23 mid-Holocene periods (Korty et al., 2012a,b). These have been unable to analyse simulated
24 tropical cyclones directly, due to the unavailability of six-hourly data throughout the
25 atmosphere in the data archive. Instead those studies (and the present one) look at indices
26 describing how favourable the climate state is for tropical cyclogenesis. For the LGM, Korty
27 et al. (2012a) observed higher genesis potential relative to the preindustrial era on the global
28 mean. They also found robust regional changes, for example a shift in potential genesis from
29 the North Atlantic to the western North Pacific (Korty et al., 2012a). For the mid-Holocene
30 era, Korty et al. (2012b) demonstrated that the difference in distribution of the top-of-
31 atmosphere (TOA) radiation in comparison to the preindustrial control altered the seasonal
32 cycle of potential intensity (maximum achievable storm strength) in the Northern

1 Hemisphere. There was mixed response in TC genesis potential for the mid-Holocene relative
2 to the preindustrial period: the northern hemisphere becomes slightly less favourable for TC
3 activity, whilst the southern hemisphere becomes more favourable.

4

5 This study aims to investigate if similar behaviours are seen in the subsequent generation of
6 PMIP; namely the PMIP3 model ensemble. The related Pliocene ensemble (PlioMIP) is
7 included to investigate whether there is a robust response to carbon dioxide concentrations. A
8 further objective is to explore how factors associated with TC genesis in these palaeoclimates
9 (equilibrium states) relates to those under future simulations (transient scenarios).

10

11 The various model simulations used in this study are described in Section 2. The calculation
12 of genesis potential index (GPI) that underpins this study will be presented in Section 3 of this
13 paper along with its limitations. Section 4 consolidates the results from the GPI analysis of the
14 various palaeoclimates derived from the GCM ensembles. Unfortunately measures of storm
15 frequency, intensity and landfall are not possible with this methodology and so cannot be
16 analysed. A discussion of how the climatology in the Pliocene, LGM and mid-Holocene may
17 affect TC genesis potential relative to the preindustrial period will be covered in section 5, as
18 will the effects of elevated carbon dioxide concentration on GPI. Section 6 will summarise
19 this paper's key findings.

20

21 **2 Climate Simulations**

22 The Pliocene Model Intercomparison Project (PlioMIP), which complements the LGM and
23 the mid-Holocene aspects of the PMIP Phase 3 (PMIP 3), coordinates the efforts of various
24 international climate modelling teams to quantify uncertainties in model outputs using the
25 average interglacial conditions of the mid-Piacenzian (hereafter known as Pliocene) climate
26 boundary conditions between 3.29 Ma and 2.97 Ma (Haywood et al. 2011).

27

28 Nine coupled climate models participated in PlioMIP (Haywood et al. 2013), although only
29 five are analysed here. The GCM dataset selection for this study is largely dependent on data
30 availability for the large-scale climatic variables, such as the atmospheric temperature and

1 humidity profile, from the PlioMIP project for the Pliocene epoch. PMIP3 data for the LGM,
2 mid-Holocene and preindustrial are taken from the same GCM that is used in the Pliocene
3 simulation. In one instance, a different GCM from the same model family (MIROC) was used
4 in the PlioMIP compared to the rest of PMIP. Here a preindustrial control from that particular
5 GCM generation was used for comparison. A similar approach is taken for HadCM3, where
6 intriguingly the PlioMIP and PMIP preindustrial simulations show different properties
7 (perhaps an undocumented model improvement has been included in the PlioMIP version).
8 Data for the representative concentration pathway 8.5 W/m² (RCP 8.5) is likewise analysed as
9 an example of a future elevated carbon dioxide concentration scenario. The GCMs that have
10 been included for this study are outlined in Table 2.

11
12 Throughout this work, the genesis potential index presented has been calculated using
13 monthly climatological values of the climate model variables (rather than computing a
14 climatology of monthly varying GPI). This approach was adopted for pragmatic reasons,
15 although Korty et al. (2012a) suggest the impacts on the results are small. We investigated the
16 sensitivity of this choice for a single GCM and also found it to be minor. In situations where a
17 pre-computed monthly climatology of a particular epoch is not available on the Earth System
18 Federation Grid, a 50-year time-slice from the end of the period of interest is used to generate
19 the monthly climatology data so as to minimise stochastic effects, model drift and internal
20 variability. The number of vertical levels used by each model are given in Table 2. However,
21 as the models have a hybrid vertical coordinate whilst the data in the CMIP archive is
22 provided on constant pressure levels, the actual number of levels used for the PI computation
23 is often less. Nonetheless, all models have data from well up into the stratosphere. The GPI is
24 only calculated between 30°S and 30°N and the cumulative values given in this study
25 represent the integral over this latitude band. Whilst this assumes that conditions favourable
26 for cyclogenesis only ever occur within that band, the spatial distributions in seen in our
27 results indicate the assumption is valid. The ensemble mean is obtained by first bi-linearly
28 interpolating the individual model fields onto the coarsest-resolution grid (HadCM3 in this
29 case) and then averaging. Any missing data (i.e. land) is infilled prior to the regridding and
30 then the coarsest-resolution land-sea mask reapplied subsequently.

31

1 Calculating the range associated with internal variability in GPI is challenging. Here ten 10-
2 year time-slices are taken from a hundred year dataset of the preindustrial dataset of each
3 model. The standard deviation (SD) is found to be within 1-3% of the preindustrial (PI) TC
4 genesis annual frequencies simulated across the five GCMs (Table 2). It is not clear to us how
5 the longer-term internal variability (i.e. that associated with climatologies) relates to this
6 estimate. Intuitively one may expect it to be smaller, as the climatology averages over more
7 ENSO cycles than the decadal estimates. However, research into the interannual applicability
8 of large-scale storm-related metrics (such as GPI) suggest that they underestimate the
9 variability (Villarini and Vecchi, 2012).

10 **3 Genesis Potential Index**

11 The use of “genesis potential” is particularly useful for addressing cyclone-related questions
12 with climate models. The grid resolution of most GCMs is not sufficiently refined to simulate
13 mesoscale processes required to adequately capture tropical cyclones. Many studies have used
14 genesis potential indices as a less computationally intensive and more practical approach to
15 describe how favourable climate conditions are for the tropical cyclogenesis (Bruyère et al.
16 2012; Camargo et al. 2007; Emanuel and Nolan 2004; Korty et al. 2012a, b; Menkes et al.
17 2012; Tippett et al. 2011).

18

19 Gray (1975) pioneered work on a genesis potential index (GPI) by demonstrating the use of
20 selected atmospheric properties characterise climatic conditions that are favourable for
21 cyclone genesis. Following subsequent developments (Emanuel and Nolan, 2004; Emanuel et
22 al., 2008) the use of a GPI is considered state-of-the-art (Tippett et al. 2011). It incorporates
23 the potential intensity theory (Emanuel 1988; Holland 1997) that evaluates the maximum
24 wind speed that may be attainable using the available thermodynamic energy imparted from
25 the atmospheric environment and the sea surface (Camargo et al. 2013) to the TC. It is worth
26 noting that just because a genesis potential index that performs well in the modern climate, it
27 may not adequately capture the actual response of cyclogenesis to a changed climate
28 (Camargo et al., 2014). In the following description, we must assume that the GPI index
29 described below - derived from modern observations – works as a proxy for changes in
30 cyclogenesis in past climate simulations as well.

31

1 The GPI proposed by Emanuel and Nolan (2004) and subsequently developed by Emanuel et
2 al. (2008) serves to synergise the thermodynamic and kinematic factors affecting TC genesis
3 into a single index. With the aim of facilitating comparison with previous investigations into
4 palaeoclimate cyclone genesis, the “clipped vorticity” version of the GPI employed by Korty
5 et al (2012a, b) has likewise been adopted for this study:

$$GPI = \frac{b[\min(|\eta|, 4 \times 10^{-5})]^3 [\max(PI - 35, 0)]^2}{\mathcal{X}_m^{\frac{4}{3}} [25 + V_{shear}]^4}$$

7 (1)

8 Here, η represents the absolute vorticity computed at the 850hPa level (Nolan and Rappin
9 2008), V_{shear} is the 200-850 hPa wind shear value, \mathcal{X}_m is the moist entropy deficit. PI is the
10 maximum potential intensity a TC can theoretically achieve (Emanuel 1988). Due to the
11 inherent biases in convection schemes and parameterisations employed by GCMs, the global
12 annual total TC genesis has to be calibrated (Emanuel et al. 2008). b is therefore an
13 empirically derived normalisation factor that calibrates the GPI to achieve preindustrial
14 cumulative annual cyclone genesis frequencies of the ninety storms observed per year in the
15 modern period. This approach means that the percentage changes in local GPI for each model
16 will be reflected in the ensemble mean. Previous work (Korty et al., 2012a,b) used a constant
17 value of b across the ensemble. Such an approach would mean that small absolute changes in
18 GPI in modelled conditions biased against cyclone genesis contribute less to the ensemble
19 mean picture. It is not clear which approach is the most relevant in this context.¹

20
21 Wind shear and absolute vorticity are the two kinematic factors included in the GPI, while
22 potential intensity and moist entropy deficit are both thermodynamic factors (Korty et al.
23 2012a). Wind shear, which is the vertical shear of the horizontal winds between the upper and
24 lower troposphere, causes asymmetries in the developing cyclone which results in the
25 ventilation of the upper level warm core through the flushing of relatively cooler and drier air

¹ In the initial submission of this manuscript the constant b approach of Korty et al. (2012a,b) was used. We therefore invite the reader to compare the present figures to those visible from the open review stage to observe the impact of this choice on the ensemble mean patterns.

1 from the top (Frank and Ritchie 2001). Stronger wind shear therefore influences inflow
2 dynamics and weakens cyclone formation (Riemer et al. 2013). While noting caveats where
3 such two-level vector differentials may be inadequate to describe the resultant wind shear in
4 some scenarios (Velden and Sears 2014), this study defines the wind shear as the difference
5 between the 200hPa and 850hPa winds given its ease of computation.

6

7 Meanwhile, the vorticity serves as a spin-up mechanism that initiates cyclone formation in a
8 recirculating flow that is quasi-closed in the lower troposphere. Taking the analogy of a
9 protective pouch (Dunkerton et al., 2009), the quasi-closed streamlines surround the enhanced
10 vorticity while nurturing the thermodynamic and convective processes that favour TC
11 development (Tory et al. 2012). Tippett et al. (2011) observed that vorticity has a greater
12 influence on cyclone formation at lower latitudes, and other factors play a greater role at
13 higher latitudes. They also propose incorporating a “clipped vorticity” diagnosis in place of
14 absolute vorticity in the GPI, so as to moderate its response in over-estimating TC genesis for
15 the sub-tropics. Potentially, the clipping threshold (set at $4 \times 10^{-5} \text{ s}^{-1}$ in eq. 1) may have varied
16 in the past through large-scale changes in the atmosphere circulation. Sensitivity analysis
17 performed indicates that changes in the clipping threshold appear to have little substantive
18 impact on the resulting change in GPI for this study (not shown).

19

20 The non-dimensional term (\mathcal{X}_m) measures the moist entropy difference between the mid-
21 troposphere and the boundary layer that is derived from asymmetric cyclone models
22 (Emanuel 1995b), as shown below:

23

$$\mathcal{X}_m = \frac{s_b - s_m}{s_o^* - s_b} \cong \frac{s^* - s_m}{s_o^* - s_b}$$

24

(2)

25 s_m , s_b and s_o^* represent the moist entropies of the mid-troposphere layer, boundary layer, and
26 the sea surface saturation entropy respectively. Taking the assumption that the lapse rate of
27 the tropical atmosphere is largely moist adiabatic (Emanuel et al. 2008), s^* which is the
28 saturation entropy above the boundary layer, is assumed to be constant throughout the
29 atmospheric column. This allows the numerator term in Eq. (2) to be evaluated at 600hPa,

1 which is taken to represent the mid-troposphere as defined by Emanuel (1994). s_b and s_o^* are
2 calculated at 925 hPa for the boundary layer and at the sea surface respectively. We use the
3 Bolton (1980) equation to calculate the saturation vapour pressures needed for the Emanuel
4 (2008) definition of moist entropy. Physically, a larger \mathcal{X}_m signifies a longer duration needed
5 for an initial perturbation to moisten the middle troposphere before intensification occurs
6 (Emanuel et al. 2008).

7

8 Taking on the analogy of a cyclone's evolution process as equivalent to Nature's Carnot
9 engine (Emanuel 1988, 1991), the potential intensity diagnostic derived by Bister and
10 Emanuel (1998, 2002) that takes into account the effects of dissipative heating is:

11

$$Potential\ Intensity\ (PI) = \sqrt{\frac{C_k}{C_d} \frac{SST}{T_o} (CAPE^* - CAPE_b)}$$

12

(1)

13 C_k and C_d are the surface exchange coefficients for enthalpy and momentum. Its ratio could
14 range between 0.1 to 1.3 (Montgomery et al. 2010) and is likely between 0.75 and 1.5 for
15 observed cyclones (Emanuel 1995a). In this study, a ratio of $C_k/C_d=1$ is taken to allow for
16 ease of comparison with previous work that used a similar assumption (Korty et al. 2012a). T_o
17 is an entropy-weighted mean temperature of the outflow. The convective available potential
18 energy ($CAPE^*$) describes an air parcel of maximum wind intensity that has been earlier
19 saturated at the sea surface, while $CAPE_b$ describes a boundary layer air parcel which has
20 been isothermally lowered from an equivalent air parcel of maximum wind intensity. Climate
21 variables that are required for the potential intensity calculation include SST and pressure of
22 the sea surface, as well as the humidity and temperature profile of the atmospheric column.
23 Potential intensity in this study is approximated by using a commonly applied algorithm
24 (Bister and Emanuel, 2002). Garner (2015) provides a detailed discussion of the relationship
25 between potential intensity and CAPE, as well as investigating the errors associated with the
26 approximations inherent in the algorithm.

27

1 Having described both the genesis potential index and potential intensity, it is necessary to
2 stress what these metrics can and, more importantly, cannot measure. Potential intensity
3 assesses the environmental conditions and calculates the maximum strength a storm could
4 achieve if it extracted all the available energy. It is not a measure the actual cyclone intensity,
5 which is often substantially smaller. The GPI is a measure of how favourable local
6 atmospheric conditions are for tropical cyclone genesis to occur. A high GPI does not mean a
7 storm will form at the location – other criteria such as an initial disturbance to act as storm
8 seed are also needed. Changes in potential intensity and GPI combined provide useful
9 information about how favourable altered climates would have been for tropical cyclones to
10 form and strengthen (Camargo et al., 2014). However, they do not give us any information
11 about many interesting aspects of tropical cyclones, such as their distribution, tracks, size,
12 intensity or the ocean mixing they cause.

13 **4 Results**

14 **4.1 Potential Intensity**

15 In the tropical region, the Pliocene saw higher SSTs by about 2 °C relative to the preindustrial
16 control (and the mid-Holocene), while SSTs were lower by about 2 °C at the LGM (Figure 1).
17 Korty et al. (2012a) suggest the 55 ms⁻¹ potential intensity contour coincides with the region
18 where deep convection, and hence tropical cyclogenesis, is possible. Interestingly the
19 locations of the 55 ms⁻¹ potential intensity contour appears to be relatively insensitive to these
20 wholesale SST changes. For example, the contour in the North Pacific is associated with SSTs
21 ranging from 26 °C during the Pliocene to 22 °C at the LGM. All climates show a rapid drop
22 in potential intensity near 30° latitude, suggesting it is valid to constrain the analysis to within
23 this latitude band.

24

25 During the Pliocene, there is a reduction in potential intensity for the North Atlantic, despite
26 an SST increase in the same region (Figure 1b). This supports research showing that absolute
27 SST by itself can be an inadequate indicator of storm strength (Vecchi et al., 2008). Whilst,
28 this may appear to depart from early understanding of threshold SST values (e.g. 26 °C) in
29 influencing cyclone genesis (Palmen 1948), it rather underscores the importance of other
30 factors, such as atmospheric humidity and upper troposphere outflow temperature relative to

1 the SST, that jointly determine the magnitude of energy available to a tropical cyclone
2 (Emanuel, 1998).

3 **4.2 Preindustrial**

4 The preindustrial era serves as a useful reference climate as it is before Earth's environment
5 came under substantial anthropogenic influence, especially over the tropical oceans (Lewis
6 and Maslin, 2015). Figure 2 illustrates the Genesis Potential Index (GPI) seen in the various
7 GCMs in their preindustrial simulations. After Korty et al (2012a,b), the northern hemisphere
8 shows cyclone genesis potential averaged over the peak storm periods of July, August,
9 September and October (JASO), while the southern hemisphere corresponds to the peak storm
10 period of January, February, March, April (JFMA). Monthly storm genesis will be discussed
11 in section 4.6.

12

13 The GPI distribution of the various GCMs compares favourably with the outcomes from
14 similar model analysis by Camargo (2013) for the preindustrial period, despite the use of
15 slightly different genesis potential indices. All models simulate conditions favourable for
16 cyclone genesis from the eastern and western Pacific in the northern hemisphere during
17 JASO, as well as the eastern Pacific near the South Pacific Convergence Zone (SPCZ) during
18 JFMA. Stronger GPI in the southern Indian Ocean is found during JFMA, with limited
19 genesis potential in the northern Indian Ocean during JASO apart from some areas such as the
20 northern Bay of Bengal. The North Atlantic features some high genesis potential at the deep
21 and sub-tropics, but the South Atlantic shows almost negligible potential for TC genesis.
22 These features are all shown in observations of actual tropical cyclone genesis (Knapp et al.,
23 2010). It should however be remembered that the genesis potential index is optimised
24 precisely to replicate these spatial and seasonal characteristics.

25

26 However the various models do show some biases. CCSM4 and IPSL-CM5A-LR exhibit a
27 band of GPI in the North Pacific that is too zonal. The East-West split in HadCM3, FGOALS-
28 G2 and MIROC-ESM is more representative of Pacific observations. However both HadCM3
29 and MIROC-ESM have a West Pacific development region that is not sufficiently favourable
30 for cyclogenesis and is constrained to the coastal regions. While IPSL-CM5A-LR suggests

1 that the central-western Pacific would have its most favourable conditions for cyclone genesis,
2 MIROC-ESM and HadCM3 show their greatest GPI in the north-eastern Pacific. FGOALS-
3 G2 shows a relatively uniform strength of genesis potential across all the oceans, apart from
4 an area of increased intensity in the eastern North Pacific and Philippine Sea. The genesis
5 potential also stretches across a greater area in FGOALS-G2 relative to the other models.
6 There appears insufficient GPI in the North Atlantic in nearly all the models, although
7 CCSM4 and MIROC-ESM are especially weak. The Southern Hemisphere has a band of high
8 GPI that is again a little too zonal in nature, although the southerly curvature in MIROC-ESM
9 is commendable. This feature arises from the bias in the model representation of the SPCZ
10 (Saint-Lu et al., 2015).

11
12 The ensemble mean (figure 2f) averages out the several of the biases seen by individual
13 models. This PMIP3 preindustrial ensemble reveals highly similar distribution of genesis
14 potential index for regions such as the North Atlantic, Pacific and Indian oceans in
15 comparison with the 0ka genesis potential from Kerty et al. (2012a) calculated using PMIP2
16 data from seven GCMs. In both instances, the highest intensity of genesis potential is located
17 between the 10°-20° latitude belts of the respective peak storm periods of both hemispheres,
18 and both are of comparable cumulative genesis magnitude of between 3-5 occurrences m⁻²
19 month⁻¹ (not shown). The preindustrial climate thus exhibits consistency in favourable
20 cyclogenesis locations between the PMIP3 and PMIP2 simulations (note however that
21 HadCM3 occurs in both ensembles and all other PMIP3 models have an earlier generation
22 entered in PMIP2).

23 **4.3 Mid-Holocene**

24 The key difference between the mid-Holocene and preindustrial climate lies in the changes in
25 solar insolation arising from different angular precession (Table 1). As a result, the northern
26 hemisphere receives proportionally greater insolation during its storm season compared to the
27 southern hemisphere. The summer and annual mean insolation for the high latitudes in both
28 hemispheres is also increased (Braconnot et al. 2007).

29

1 These insolation changes drive responses in simulated genesis potential index across the five
2 models (Figure 3). The magnitude of the response in all models is similar. HadCM3 and
3 MIROC-ESM show a widespread reduction of genesis potential in the northern hemisphere
4 compensated for by an increase in the southern hemisphere. The response of IPSL-CM5-LR
5 and CCSM4 bear similarities to each other in that their bands of GPI in the North Pacific
6 become more zonal (as visible by the dipole patterns in Fig. 3).

7

8 The ensemble genesis potential for the mid-Holocene (Figure 4a) shows a largely similar
9 distribution as the preindustrial period (Figure 2f), although a broadly coherent pattern of GPI
10 change is observed (Figure 4b). The southern hemisphere exhibits a weak increase in GPI
11 from mid-Holocene over preindustrial, except for pockets around Northern Australia that
12 show a stronger increase. A northward shift in GPI is noticeable in the eastern North Pacific,
13 unsurprisingly associated with the local shift in ITCZ. This shift in the ITCZ would be
14 expected to not only impact the genesis of storms (Merlis et al, 2013) but also their intensity
15 (Ballinger et al, 2015). A slight decrease in genesis potential is seen in the North Atlantic.

16

17 There is a good agreement across the ensemble on the sign of the mid-Holocene change in
18 most areas amongst the five GCMs (Figure 4c). There is a general decrease in GPI in the
19 northern hemisphere, and an increase in GPI as one moves polewards in the southern
20 hemisphere. Although several regions show strong agreement for increased GPI, such as the
21 South-East Pacific and South Atlantic, these are regions of minimal cyclone occurrence at
22 present (Knapp et al., 2010) and should not be interpreted as having storms in the mid-
23 Holocene.

24

25 The results for the mid-Holocene using these PMIP3 models bear strong similarities with
26 findings from Kerty et al. (2012b) that detail cyclone genesis potential using an ensemble
27 from ten GCMs from PMIP2. The magnitude and distribution of genesis potential share
28 similar patterns across all oceans. Nonetheless this study simulates a slightly weaker genesis
29 potential for the western South Indian Ocean and the South Atlantic, as well as a slightly
30 weaker increase in genesis potential for mid-Holocene over preindustrial in both hemispheres.

1 The model agreement (Figure 4c) is also similar to that of Korty et al. (2012b) with both
2 showing an anvil shape area of reduced GPI in the central North Pacific.

3 **4.4 Last Glacial Maximum (LGM)**

4 During the LGM, the tropics experienced cooling of 5 °C to 2 °C over land, while most of the
5 tropical surface ocean did not encounter cooling beyond 2 °C especially in the southern
6 hemisphere (Waelbrook et al. 2009). The LGM mean tropical SST from the five GCMs in this
7 study during the peak storm period is 2.0 °C cooler than preindustrial. Simulated genesis
8 potential responses for the LGM show both variations spatially and across the ensemble
9 (Figure 5). CCSM, HadCM3 and MIROC show generally stronger potential genesis, while
10 FGOALS and IPSL show a weakening in genesis potential relative to preindustrial. All of the
11 models show some form of compensation, indicative of shifts in the relative dominance of the
12 TC formation locales.

13

14 The ensemble genesis potential for the LGM (Figure 6a) shares again, at a first glance, a
15 similar distribution with the preindustrial. However, it exhibits greater intensity of genesis
16 potential in the central North Pacific and near the SPCZ (Figure 6b). The central-eastern
17 South Indian Ocean shows decrease in genesis potential along 10°S, whilst the South Pacific
18 sees an increase. Some of this shift in GPI is related the increased land exposure in the
19 Maritime continent at the LGM – a feature that is treated somewhat differently between the
20 models (observe the land masks in Fig 5). There are slight decreases of genesis potential
21 observed in the North Atlantic.

22

23 There is some model agreement (Figure 6c) focussed around the largest changes in genesis
24 potential in the LGM period for most oceans relative to preindustrial. The North Atlantic
25 exhibits a very robust decrease in genesis potential that spreads over Central America into the
26 eastern North Pacific. This is likely a response to the imposition of the Laurentide ice sheet
27 and its impact on the regional circulation. There appears to be a dipole pattern in the Indian
28 Ocean (most noticeable in Figure 6c), although it is not as robust. This is likely an expression
29 of the alteration in Walker Circulation (DiNezio et al, 2011), whose fidelity varies across
30 models depending on their parameterisations and boundary conditions (DiNezio and Tierney,

1 2013). These patterns of the model agreement are qualitatively similar to those seen in the
2 PMIP2 experiments (Korty et al. 2012a), yet show more consistency across the ensemble.

3

4 **4.5 Pliocene**

5 The Pliocene is a warmer climate compared to preindustrial (Dowsett et al, 2010; Haywood et
6 al., 2013), with the area-averaged tropical SST from the five GCMs in this study over the
7 peak storm season being 1.7 °C warmer. In terms of the GPI difference from preindustrial
8 (Figure 7), most models suggest a mixed response in the direction of change for various
9 oceans, apart from MIROC that shows only a limited change. The majority of models indicate
10 a decrease in genesis potential for the North Atlantic and South Indian oceans. In the North
11 Pacific Ocean, the majority of models suggest a decrease in genesis potential in the eastern
12 development region, but appear to have mixed responses for the western region and the
13 SPCZ.

14

15 As for the preindustrial, the conditions most favourable to cyclone genesis in the Pliocene
16 ensemble mean can be found in the eastern and western areas of the North Pacific, the SPCZ
17 and central region of the South Pacific, as well as the north-western corner of the South
18 Indian Ocean (Figure 8a). In terms of the difference in genesis potential between the Pliocene
19 and preindustrial periods (Figure 8b), the North Atlantic, North Pacific, and South Indian
20 oceans and the SPCZ region experience a decline in favourable cyclogenesis conditions. It is
21 worth noting that HadCM3 simulates a reduction in GPI for nearly all regions of observed
22 cyclogenesis (Figure 7c).

23

24 This large-scale pattern appears to be robust as most models suggest a general decrease in
25 genesis potential for the Pliocene relative to the preindustrial for most oceans (Figure 8c),
26 although the magnitude of change might be small in areas - such as the South Atlantic and
27 eastern South Pacific. There appears to be weaker model agreement on the sign of change for
28 the subtropical latitudes for the Pacific and Indian oceans in both hemispheres, although a
29 slight increase in genesis potential may be expected.

30

1 4.6 Genesis Frequency

2 Figure 9 illustrates the cumulative annual, global genesis potential index generated from the
3 five GCMs across the various palaeoclimates as a percentage of the preindustrial. Remember
4 each preindustrial GPI field is normalised such that this sum equals 90 – roughly akin to the
5 observed number of storms formed globally each year in the modern climate. The ensemble-
6 mean annual, global totals for the Pliocene, LGM and mid-Holocene are determined to be
7 89%, 97% and 101% of the preindustrial respectively.

8

9 Estimating the natural variability (or more strictly ‘internal variability’) of an ensemble mean
10 number is problematic. As a pragmatic measure, we take that of the model with the highest
11 internal decadal variability (HadCM3) - giving a standard deviation (σ) of 2.9%. Given that
12 the ensemble cumulative values are generally within the standard measure of 2σ (Haywood et
13 al. 2013), the cumulative GPI for both the LGM and mid-Holocene is considered to have not
14 deviated significantly from the preindustrial era. Whilst the ensemble mean value for the
15 Pliocene is statistically significant by this metric, the magnitude of the reduction is in fact
16 driven primarily by the HadCM3 member (the ensemble average without it is 98% of the
17 preindustrial). The assumption of a Gaussian distribution inherent in this metric of
18 significance is clearly not valid for this ensemble. It is therefore not clear we can consider the
19 reduction seen in Pliocene ensemble as robust feature. This is especially true in light of the
20 uncertainty in the internal variability measure itself discussed in section 2.2. Despite this note
21 of caution, it is worth remembering that these GPI changes appear of a similar magnitude to
22 those seen in future projections (Camargo, 2013; Emanuel, 2013), which are anticipated to
23 have important consequences.

24

25 In Figure 10, the northern hemisphere peak in JASO appears consistent across the various
26 epochs, as does the southern hemisphere’s peak in JFMA. This justifies the choice of the peak
27 storm seasons for the respective hemisphere as presented here. Previous work from Korty et
28 al. (2012a, b) using PMIP2 data showed a stronger peak from the southern hemisphere
29 relative to the north, while this study suggests a stronger northern hemisphere peak. This
30 suggests that the PMIP3 simulations may have improved accuracy in describing present day

1 trends of northern hemisphere for conditions more conducive for cyclone genesis (Gray 1968;
2 Klotzbach 2006; Webster et al. 2005).

3
4 Korty et al. (2012a) found a slight increase in cumulative GPI at the LGM in the previous
5 generations of models. This ensemble shows a marginal reduction in this metric, yet there is
6 substantial spread between the models themselves (Fig. 9). The reduced TC genesis potential
7 index associated with the warm Pliocene conforms to the Knutson et al. (2010) view of future
8 behaviour. It does differ from the sole prior Pliocene TC study (Fedorov et al 2010), both in
9 results and approach. A discussion of the two pieces of work follows in section 5.1.

10

11 For the mid-Holocene epoch, a salient increase in October activity is observed by Korty et al.
12 (2012b), which has been attributed to a delayed SST response from the TOA insolation
13 forcing, resulting in a shift of the northern hemisphere storm season. However, such a feature
14 is not observed in this study. Annual SST changes are found to have varied minimally relative
15 to the preindustrial (Figure 1), suggesting that the ocean component during the mid-Holocene
16 may play a lesser role in comparison to the Pliocene and LGM epochs where more substantial
17 SST changes are observed.

18 **5 Discussion**

19 During the Pliocene and LGM, changes in carbon dioxide led to sea surface temperature
20 (SST) changes throughout the tropics, yet the potential intensity of TCs are observed to be
21 relatively insensitive to these changes (Figure 1). The cumulative genesis potential index
22 (taken as proxy for global storm numbers per year) is likewise found to be fairly consistent
23 across the various palaeoclimates. Despite disagreement about the change of global annual
24 TC frequency (Figure 9), there is some model consensus on the spatial patterns of tropical
25 cyclogenesis change. These changes may be attributable to changes in large scale atmospheric
26 properties such as carbon dioxide levels, altered topography and orbital forcing.

27

28 The key difference in forcing between the mid-Holocene and preindustrial lies in the orbital
29 parameters (Table 1). Solar insolation received in the northern hemisphere is enhanced
30 relative to the southern hemisphere as a result of the altered precession (Braconnot et al.
31 2007). There is a slight tropospheric warming in the northern hemisphere for the middle and

1 high latitudes as a consequence of this, while general tropospheric cooling is found in the
2 tropical region and the southern hemisphere. Increased genesis potential is observed during
3 the mid-Holocene in the southern hemisphere, along with slight reduction in the northern
4 hemisphere (Figure 4c). This is associated with higher entropy deficit in the northern
5 hemisphere which would act to hinder cyclone genesis compared to the southern hemisphere
6 (not shown) as found by Korty et al. (2012b). The potential intensity increases very slightly at
7 all latitudes (not shown).

8

9 Carbon dioxide, being a well-mixed greenhouse gas, causes globally coherent temperature
10 changes in contrast to orbital forcing. The Pliocene represents a period of elevated carbon
11 dioxide concentration resulting in a warmer climate relative to the preindustrial period, while
12 the LGM era experienced an opposite cooling effect arising from lower carbon dioxide levels
13 present at that time. Korty et al. (2012a) emphasise the fact that conditions at the LGM remain
14 roughly as favourable as the preindustrial for tropical cyclones. They discuss the slight
15 increase in favourably brought about local changes in the entropy deficit and wind shear terms
16 in PMIP2. The most robust changes in GPI in the present ensemble occur in the Atlantic and
17 appear stronger than found by Korty et al. (2012a). The ultimate cause of this difference is
18 likely the inclusion of altered ice-sheets in the PMIP3 vs PMIP2 experiments (Abe-Ouchi et
19 al., 2015). This results in a small cooling of SSTs (>0.5 °C) stretching from the Caribbean to
20 West Africa and consequently a change in potential intensity that less is than seen by Korty et
21 al. (2012a).

22

23 In response to the greenhouse gas driven warming seen in the Pliocene experiments (Hill et
24 al., 2014), a general decrease is observed in genesis potential in the convergence zones in both
25 the northern hemisphere and southern hemispheres (Figure 7, 8b). The PlioMIP simulations
26 have a weaker Hadley and Walker circulation that results in a broadening of the Inter-tropical
27 Convergence Zone (ITCZ; Contoux et al. 2012). Kamae et al. (2011) show that Equatorial
28 specific humidity increases in the lower troposphere and decreases in the mid-troposphere
29 arising from a weakened ascent of the Walker circulation in the PlioMIP simulations.
30 Convective processes are curtailed leading to an associated increase in moist entropy deficit
31 (not shown) which leads to the general decrease in GPI within the Pliocene simulations.

1 **5.1 Possible sea surface temperature biases and missing feedbacks**

2 Prior work looking at tropical cyclones in the Pliocene (Fedorov et al., 2010) shows a rather
3 different behaviour than that found here. The two studies approach the Pliocene climate and
4 its tropical cyclones from alternate standpoints. By summarising both approaches, we hope
5 here to allow readers to consider their respective merits.

6

7 Fedorov et al. (2010) start with proxy SST observations from the early Pliocene (~4 Ma),
8 which imply much weaker tropical SST gradients both meridionally (Brierley et al., 2009)
9 and zonally (Wara et al., 2009). Although there has been some criticism of the
10 palaeothermometers (O'Brien et al., 2014; Zhang et al., 2014a); this does not affect the
11 estimates of reduced SST gradients (Ravelo et al., 2015; Brierley et al., 2015; although note
12 the response of Zhang et al., 2014b). Coupled climate models seem unable to replicate this
13 climate state (Fedorov et al., 2013). Fedorov et al. (2010) use an atmosphere-only model
14 driven by a prescribed 'Pliocene' SST field (Brierley et al., 2009) to create inputs for a
15 statistical-dynamical downscaling model (Emanuel et al., 2008). The statistics of the tropical
16 cyclones directly simulated by the downscaling model were analysed and show a substantial
17 increase of tropical cyclones across the globe. Fedorov et al. (2010) then focus on the increase
18 in the central Pacific and suggest that these storms could be part of a feedback that maintains
19 the weak zonal SST gradient on the Equator.

20

21 This study uses simulations from the PlioMIP experiment that aims to investigate systematic
22 biases between the palaeobservations and modelled climates of the Pliocene (Haywood et al.
23 2011). This experiment focuses on ~3 Ma and finds many similarities on global-scale
24 (Haywood et al, 2013). There are some regions with substantial mismatch across the
25 ensemble however, most notably the high latitude North Atlantic and Tropical Pacific. As a
26 whole this ensemble does not show any change in the zonal SST gradient, something true of
27 every model in the subset used here (Brierley 2015). Aside from the limitation of using a
28 genesis potential index, the present study may therefore include a systematic bias in its
29 representation of the Pliocene - although it has been suggested (O'Brien et al., 2014; Zhang et
30 al., 2014a) that in fact the palaeobservations are in error. Nonetheless it is interesting that the
31 present study shows an increase in genesis potential in the central Pacific – impinging on the

1 subduction zone critical for the cyclone-climate feedback discussed by Fedorov et al. (2010).
2 Should cyclone-climate feedbacks be an important feature of the actual Earth System, then
3 systematic biases would exist across all the simulations presented here, not only the Pliocene
4 ones.

5 **5.2 Relationship to future projections**

6 Records do not currently exist to either confirm or refute the potential of the atmospheric
7 conditions simulated by this ensemble for tropical cyclogenesis. They probably never will.
8 Yet the Earth will shortly experience carbon dioxide concentrations beyond those of the
9 Pliocene period. Therefore, it is interesting to consider how the results above correspond to
10 future projections. One further motivation to do this is that the palaeoclimate simulations are
11 all equilibrium experiments, whilst the future projections are transient. It is therefore
12 anticipated that the climate change signal will be easier to detect in the palaeoclimate
13 simulations. In transient simulations, large scale forcings may not fully account for the
14 observed variability (Menkes et al. 2012), as stochastic effects may potentially account for up
15 to half of the observed variability (Jourdain et al. 2010).

16

17 The RCP8.5 scenario is used to project how GPI may develop in future. It is chosen as it is
18 the most extreme scenario and so should have the biggest signal. In this scenario, carbon
19 dioxide concentrations reach over 900 ppmv by 2100 (Collins et al., 2013); more than double
20 the level in the Pliocene simulations.

21

22 The GCMs selected in this study all show future changes in tropical cyclone count (at least as
23 estimated by the cumulative GPI) under the RCP8.5 transient scenario (Figure 11). Yet these
24 trends are not consistent between the models. Note that HadCM3 has not contributed results
25 for RCP8.5, so a later generation of the model (HadGEM2) has been substituted. Two models
26 suggest an increase in cumulative GPI, while three models suggest a decrease, resulting in an
27 ensemble mean with a trend of slightly reduced cumulative GPI by 2095. The future response
28 is also seemingly inconsistent with the palaeoclimate responses in the same GCM. For
29 example, MIROC shows a decrease in the warm Pliocene and an increase during the LGM:
30 counter-intuitively it also shows an increase under RCP8.5. Efforts to detect obvious

1 relationships in across the ensemble – for example between North Hemispheric temperatures
2 and cumulative GPI – were unsuccessful (not shown).

3

4 Interestingly, the multi-model mean GPI difference between the future RCP8.5 (2071–2100)
5 scenario and historical (1971–2000) simulation from Camargo (2013) shows an opposite
6 pattern to the equilibrium Pliocene-control difference in Figure 8b of this study. The transient
7 RCP8.5 GPI difference in Camargo (2013) suggests a global increase (except for a small area
8 in the central South Pacific where a decrease is expected). Meanwhile the equilibrium
9 Pliocene-preindustrial difference in this study shows a general decrease (except for a region
10 of the central North Pacific that has an increase in GPI). The stark difference in GPI response
11 between the RCP8.5 and Pliocene therefore throws additional questions on the suitability for
12 the choice of the Pliocene as a projection of modern day greenhouse climate (Haywood et al.,
13 2009), at least in terms of cyclogenesis-related measures. Held and Zhou (2011) show that
14 TCs respond differently to the forcing directly and the resultant temperature changes. This
15 may mean that the equilibrium climates simulated by PMIP should not be compared to the
16 transient states driven by the future scenarios.

17

18 Emanuel (2013) downscaled six CMIP5 GCMs for the RCP8.5 projection, and concluded that
19 an increase in future global tropical cyclone activity might be expected. The same paper also
20 acknowledged that other modelling groups obtained contrasting results where modest
21 decreases (Knutson et al. 2010) and no robust change (Camargo 2013) in future tropical
22 cyclone activity had been detected. Emanuel (2013) and Camargo (2013) both supplement
23 their direct measures of cyclogenesis with analysis of GPI that supports the directions of the
24 changes found. Two models (CCSM4 and HADGEM2-ES) that Emanuel (2013) used for the
25 RCP8.5 scenario are also incorporated in this study, but a decreasing trend is not detected for
26 the two particular models here. Possible reasons that could account for the difference include
27 the use of a modified “clipped” vorticity GPI in this study, and a different choice of 250-850
28 hPa tropospheric wind shear in Emanuel (2013). The striking difference in genesis potentials,
29 despite a similar GCM choice, suggests that the GPI may be highly sensitive to slight
30 adjustments in the diagnostic definition.

31

1 Kossin et al. (2014) showed that the lifetime-maximum intensity of tropical cyclones is
2 migrating polewards at a rate of about one degree of latitude per decade, similar to the rate of
3 expansion of the tropics (Lucas et al. 2014). No coherent message about poleward expansion
4 of conditions favourable for cyclogenesis was found in this ensemble (not shown) and
5 changes in GPI are found largely in the 10°-20° region of both hemispheres, with minimum
6 adjustment in the sub-tropics.

7

8 **6 Conclusions**

9 The cumulative global, annual genesis potential index (a proxy for global tropical cyclone
10 frequency) is found to have been relatively constant over the range of past climates. This
11 range encompasses both greenhouse (Pliocene) and icehouse (Last Glacial Maximum)
12 climates and changing orbital forcing. These conditions are thought to represent the extremes
13 of climates Earth has experienced in the past three million years. Often the members of the
14 multi-model ensemble do not agree on the sign of the global change (Figure 9), leading to
15 high uncertainty on this headline metric.

16

17 The ensemble shows much higher levels of consistency on the regional scale, however. All
18 five models agree on less potential for cyclogenesis in the North Atlantic at the Last Glacial
19 Maximum. This is compensated for by an increased potential for cyclogenesis in the central
20 North Pacific, to a greater or lesser degree. This is a circulation response to the existence of a
21 large ice-sheet over North America. A qualitatively similar feature has been seen previously
22 (Korty et al., 2012a), but with some dependency on the ice-sheet imposed (Abe-Ouchi et al.,
23 2015). Obviously the reverse of such pattern would not be expected in future. The mid-
24 Holocene ensemble shows alterations of GPI associated with shifts in the intertropical
25 convergence zone driven by the altered incoming solar distribution. Again the results from
26 this ensemble are qualitatively similar to those from prior model ensembles (Korty et al.,
27 2012b).

28

29 One motivation for studying past climate tropical cyclone response was to investigate its
30 relationship to future projections. The genesis potential under the RCP8.5 scenario was
31 computed and contrasted with the palaeoclimate response. There is no simple relationship that

1 emerges between cumulative GPI and global temperature. This result implies that changes in
2 global frequency of tropical cyclones remains much less robust than regional responses. The
3 conclusion is further strengthened by the apparent sensitivity of projected future global
4 frequency to the precise genesis potential index used – with our analysis not fully supporting
5 either the results of Emanuel (2013) nor the opposing results of Camargo (2013) despite all
6 three using the same simulations.

7

8 **Acknowledgements**

9 The work was made possible through a scholarship awarded to J.H.K. from PUB, Singapore's
10 National Water Agency. The authors thank Suzana Camargo for her useful comments on GPI
11 metrics and Kerry Emanuel for his assistance, not least his release of the Potential Intensity
12 matlab routine. The assistance of Fran Bragg, Camille Contoux, Wing-Le Chan and Weipeng
13 Zheng was essential to procure the necessary Pliocene simulation files. The creation of
14 monthly climatologies for the PMIP3 simulations by Jean-Yves Peterschmitt was particularly
15 helpful. The reviewer comments from Rob Korty, Matt Huber and Tim Merlis were very
16 useful in clarifying the scope and presentation of this contribution.

17

1 References

- 2 Abe-Ouchi, A., Saito, F., Kageyama, M., Braconnot, P., Harrison, S. P., Lambeck, K., et al.
3 (2015). Ice-sheet configuration in the CMIP5/PMIP3 Last Glacial Maximum experiments.
4 *Geosci. Model Dev. Disc.*, 8(6), 4293–4336. [doi:10.5194/gmdd-8-4293-2015](https://doi.org/10.5194/gmdd-8-4293-2015)
- 5 Annan, J. D. and J. C. Hargreaves. 2013. "A new global reconstruction of temperature
6 changes at the Last Glacial Maximum." *Clim. Past* 9(1):367-376.
- 7 Ballinger, A. P., Merlis, T. M., Held, I. M., & Zhao, M. (2015). The Sensitivity of Tropical
8 Cyclone Activity to Off-Equatorial Thermal Forcing in Aquaplanet Simulations. *Journal of*
9 *the Atmospheric Sciences*, 72(6), 2286–2302. [doi:10.1175/JAS-D-14-0284.1](https://doi.org/10.1175/JAS-D-14-0284.1)
- 10 Bister, Marja and Kerry A. Emanuel. 1998. "Dissipative heating and hurricane intensity."
11 *Meteorology and Atmospheric Physics* 65(3-4):233-240.
- 12 Bister, Marja and Kerry A. Emanuel. 2002. "Low frequency variability of tropical cyclone
13 potential intensity 1. Interannual to interdecadal variability." *Journal of Geophysical*
14 *Research: Atmospheres* (1984–2012) 107(D24):ACL-26. The potential intensity algorithm
15 itself is available from <ftp://texmex.mit.edu/pub/emanuel/TCMAX/>
- 16 Bolton, D., The computation of equivalent potential temperature, *Monthly Weather Review*,
17 108, 1046-1053, 1980.
- 18 Braconnot, P., B. Otto-Bliesner, S. Harrison, S. Joussaume, J. Y. Peterchmitt, Ayako Abe-
19 Ouchi, Michel Crucifix, Emmanuelle Driesschaert, Th Fichet and C. D. Hewitt. 2007.
20 "Results of PMIP2 coupled simulations of the Mid-Holocene and Last Glacial Maximum--
21 Part 1: experiments and large-scale features." *Climate of the Past* 3(2).
- 22 Braconnot, Pascale, Yihua Luan, Simon Brewer and Weipeng Zheng. 2012. "Impact of
23 Earth's orbit and freshwater fluxes on Holocene climate mean seasonal cycle and ENSO
24 characteristics." *Climate dynamics* 38(5-6):1081-1092.
- 25 Bruyère, Cindy L., Greg J. Holland and Erin Towler. 2012. "Investigating the Use of a
26 Genesis Potential Index for Tropical Cyclones in the North Atlantic Basin." *Journal of*
27 *Climate* 25(24).
- 28 Camargo, Suzana J. 2013. "Global and Regional Aspects of Tropical Cyclone Activity in the
29 CMIP5 Models." *Journal of Climate* 26(24):9880-9902.
- 30 Camargo, Suzana J., Adam H. Sobel, Anthony G. Barnston and Kerry A. Emanuel. 2007.
31 "Tropical cyclone genesis potential index in climate models." *Tellus A* 59(4):428-443.
- 32 Camargo, Suzana J., Mingfang Ting and Yochanan Kushnir. 2013. "Influence of local and
33 remote SST on North Atlantic tropical cyclone potential intensity." *Climate dynamics* 40(5-
34 6):1515-1529.
- 35 Camargo, S. J., Tippett, M. K., Sobel, A. H., Vecchi, G. A., & Zhao, M. (2014). Testing the
36 Performance of Tropical Cyclone Genesis Indices in Future Climates Using the HiRAM
37 Model. *Journal of Climate*, 27(24), 9171–9196. <http://doi.org/10.1175/JCLI-D-13-00505.1>
- 38 Chan, W. L., A. Abe-Ouchi and R. Ohgaito. 2011. "Simulating the mid-Pliocene climate with
39 the MIROC general circulation model: experimental design and initial results." *Geoscientific*
40 *Model Development* 4(4):1035-1049.
- 41 Collins, W. J., N. Bellouin, M. Doutriaux-Boucher, N. Gedney, P. Halloran, T. Hinton, J.
42 Hughes, C. D. Jones, M. Joshi and S. Liddicoat. 2011. "Development and evaluation of an

1 Earth-system model–HadGEM2." *Geoscientific Model Development Discussions* 4(2):997-
2 1062.

3 Collins, M., Knutti, R., Arblaster, J. M., Dufresne, J.-L., Fichefet, T., Friedlingstein, P., et al.
4 (2013). Long-term Climate Change: Projections, Commitments and Irreversibility. In T. F.
5 Stocker, Q. Dahe, G.-K. Plattner, M. Tignor, S. K. Allen, J. Boschung, et al., *Climate Change*
6 *2013: The Physical Science Basis*. Cambridge, United Kingdom and New York, NY, USA:
7 Cambridge University Press.

8 Contoux, C., G. Ramstein and A. Jost. 2012. "Modelling the mid-Pliocene Warm Period
9 climate with the IPSL coupled model and its atmospheric component LMDZ5A."
10 *Geoscientific Model Development* 5(3):903-917.

11 DiNezio, P. N., Clement, A. C., Vecchi, G. A., Soden, B. J., Broccoli, A. J., Otto-Bliesner, B.
12 L., & Braconnot, P. (2011). The response of the Walker circulation to Last Glacial Maximum
13 forcing: Implications for detection in proxies. *Paleoceanography*, 26(3), n/a–n/a.
14 doi:10.1029/2010PA002083

15 DiNezio, P. N., & Tierney, J. E. (2013). The effect of sea level on glacial Indo-Pacific
16 climate. *Nature Geoscience*, 6(6), 485–491. doi:10.1038/ngeo1823

17 Dowsett, H. J., Robinson, M. M., Stoll, D. K., & Foley, K. M. (2010). Mid-Piacenzian mean
18 annual sea surface temperature analysis for data-model comparisons. *Stratigraphy*, 7, 189–
19 198.

20 Dufresne, J. L., M. A. Foujols, S. Denvil, A. Caubel, O. Marti, O. Aumont, Y. Balkanski, S.
21 Bekki, H. Bellenger, R. Benshila, S. Bony, L. Bopp, P. Braconnot, P. Brockmann, P. Cadule,
22 F. Cheruy, F. Codron, A. Cozic, D. Cugnet, N. de Noblet, J. P. Duvel, C. Ethé, L. Fairhead, T.
23 Fichefet, S. Flavoni, P. Friedlingstein, J. Y. Grandpeix, L. Guez, E. Guilyardi, D.
24 Hauglustaine, F. Hourdin, A. Idelkadi, J. Ghattas, S. Joussaume, M. Kageyama, G. Krinner,
25 S. Labetoulle, A. Lahellec, M. P. Lefebvre, F. Lefevre, C. Levy, Z. X. Li, J. Lloyd, F. Lott, G.
26 Madec, M. Mancip, M. Marchand, S. Masson, Y. Meurdesoif, J. Mignot, I. Musat, S. Parouty,
27 J. Polcher, C. Rio, M. Schulz, D. Swingedouw, S. Szopa, C. Talandier, P. Terray, N. Viovy
28 and N. Vuichard. 2013. "Climate change projections using the IPSL-CM5 Earth System
29 Model: from CMIP3 to CMIP5." *Climate Dynamics* 40(9-10):2123-2165.

30 Dunkerton, T., Montgomery, M. and Wang, Z. 2009. Tropical cyclogenesis in a tropical wave
31 critical layer: easterly waves. *Atmospheric Chemistry and Physics*, 9(15), pp.5587-5646.

32 Emanuel, Kerry. 2003. "Tropical cyclones." *Annual Review of Earth and Planetary Sciences*
33 31(1):75-104.

34 Emanuel, Kerry A. 1988. "The maximum intensity of hurricanes." *Journal of the Atmospheric*
35 *Sciences* 45(7):1143-1155.

36 Emanuel, Kerry A. 1991. "The theory of hurricanes." *Annual Review of Fluid Mechanics*
37 23(1):179-196.

38 Emanuel, Kerry A. 1994. *Atmospheric convection*: Oxford University Press.

39 Emanuel, Kerry A. 1995a. "Sensitivity of Tropical Cyclones to Surface Exchange
40 Coefficients and a Revised Steady-State Model incorporating Eye Dynamics." *Journal of the*
41 *Atmospheric Sciences* 52(22):3969-3976.

42 Emanuel, Kerry A. 1995b. "The behavior of a simple hurricane model using a convective
43 scheme based on subcloud-layer entropy equilibrium." *Journal of the atmospheric sciences*
44 52(22):3960-3968.

- 1 Emanuel, Kerry A. 2013. "Downscaling CMIP5 climate models shows increased tropical
2 cyclone activity over the 21st century." *Proceedings of the National Academy of Sciences*
3 110(30):12219-12224.
- 4 Emanuel, Kerry A. and D. S. Nolan. 2004. "Tropical cyclone activity and the global climate
5 system."
- 6 Emanuel, Kerry, Ragoth Sundararajan and John Williams. 2008. "Hurricanes and Global
7 Warming: Results from Downscaling IPCC AR4 Simulations." *Bulletin of the American*
8 *Meteorological Society* 89(3):347-367.
- 9 Fedorov, A. V., C. M. Brierley, K. T. Lawrence, Z. Liu, P. S. Dekens and A. C. Ravelo. 2013.
10 "Patterns and mechanisms of early Pliocene warmth." *Nature* 496(7443):43-49.
- 11 Fedorov, Alexey V., Christopher M. Brierley and Kerry Emanuel. 2010. "Tropical cyclones
12 and permanent El Niño in the early Pliocene epoch." *Nature* 463(7284):1066-1070.
- 13 Frank, William M. and Elizabeth A. Ritchie. 2001. "Effects of Vertical Wind Shear on the
14 Intensity and Structure of Numerically Simulated Hurricanes." *Monthly Weather Review*
15 129(9):2249-2269.
- 16 Garner, S., 2015. The relationship between Hurricane Potential Intensity and CAPE. *Journal*
17 *of the Atmospheric Sciences* 72, 141-163. doi:10.1175/JAS-D-14-0008.1
- 18 Gagan, Michael K., Linda K. Ayliffe, David Hopley, Joseph A. Cali, Graham E. Mortimer,
19 John Chappell, Malcolm T. McCulloch and M. John Head. 1998. "Temperature and surface-
20 ocean water balance of the mid-Holocene tropical western Pacific." *Science* 279(5353):1014-
21 1018.
- 22 Gent, Peter R., Gokhan Danabasoglu, Leo J. Donner, Marika M. Holland, Elizabeth C.
23 Hunke, Steve R. Jayne, David M. Lawrence, Richard B. Neale, Philip J. Rasch and Mariana
24 Vertenstein. 2011. "The Community Climate System Model Version 4." *Journal of Climate*
25 24(19).
- 26 Gordon, C., C. Cooper, C. A. Senior, H. Banks, J. M. Gregory, T. C. Johns, J. F. B. Mitchell
27 and R. A. Wood. 2000. "The simulation of SST, sea ice extents and ocean heat transports in a
28 version of the Hadley Centre coupled model without flux adjustments." *Climate Dynamics*
29 16(2-3):147-168.
- 30 Gray, William M. 1968. "GLOBAL VIEW OF THE ORIGIN OF TROPICAL
31 DISTURBANCES AND STORMS." *Monthly Weather Review* 96(10):669-700.
- 32 Gray, William M. 1975. "Tropical Cyclone Genesis in the Western North Pacific." DTIC
33 Document.
- 34 Haywood, A. M., H. J. Dowsett, M. M. Robinson, D. K. Stoll, A. M. Dolan, D. J. Lunt, B.
35 Otto-Bliesner and M. A. Chandler. 2011. "Pliocene Model Intercomparison Project
36 (PlioMIP): experimental design and boundary conditions (Experiment 2)." *Geosci. Model*
37 *Dev.* 4(3):571-577.
- 38 Haywood, Alan M., Harry J. Dowsett, Paul J. Valdes, Daniel J. Lunt, Jane E. Francis and
39 Bruce W. Sellwood. 2009. "Introduction. Pliocene climate, processes and problems."
40 *Philosophical Transactions of the Royal Society A: Mathematical, Physical and Engineering*
41 *Sciences* 367(1886):3-17.

- 1 Hill, D. J., Haywood, A. M., Lunt, D. J., Hunter, S. J., Bragg, F. J., Contoux, C., et al. (2014).
2 Evaluating the dominant components of warming in Pliocene climate simulations. *Climate of*
3 *the Past*, 10(1), 79–90. <http://doi.org/10.5194/cp-10-79-2014>
- 4 Holland, Greg J. 1997. "The maximum potential intensity of tropical cyclones." *Journal of the*
5 *Atmospheric Sciences* 54(21):2519-2541.
- 6 Jansen, Eystein, Jonathan Overpeck, Keith R. Briffa, Jean-Claude Duplessy, Fortunat Joos, V.
7 Masson-Delmotte, D. Olago, B. Otto-Bliesner, W. R. Peltier and and S. Rahmstorf.E. 2007.
8 "Paleoclimate. Climate Change 2007: The Physical Science Basis. Contribution of Working
9 Group I to the Fourth Assessment Report of the Intergovernmental Panel on Climate Change,
10 eds S Solomon et al." Cambridge University Press, New York City.
- 11 Jourdain, Nicolas C., Patrick Marchesio, Christophe E. Menkes, Jérôme Lefèvre,
12 Emmanuel M. Vincent, Matthieu Lengaigne and Fabrice Chauvin. 2010. "Mesoscale
13 Simulation of Tropical Cyclones in the South Pacific: Climatology and Interannual
14 Variability." *Journal of Climate* 24(1):3-25.
- 15 Kamae, Youichi, Hiroaki Ueda and Akio Kitoh. 2011. "Hadley and Walker Circulations in the
16 Mid-Pliocene Warm Period Simulated by an Atmospheric General Circulation Model."
17 *Journal of the Meteorological Society of Japan. Ser. II* 89(5):475-493.
- 18 Klotzbach, Philip J. 2006. "Trends in global tropical cyclone activity over the past twenty
19 years (1986–2005)." *Geophysical Research Letters* 33(10):L10805.
- 20 Knapp, K. R., Kruk, M. C., Levinson, D. H., Diamond, H. J., & Neumann, C. J. (2010). The
21 International Best Track Archive for Climate Stewardship (IBTrACS). *Dx.Doi.org*, 91(3),
22 363–376. doi:10.1175/2009BAMS2755.1
- 23 Knutson, Thomas R., John L. McBride, Johnny Chan, Kerry Emanuel, Greg Holland, Chris
24 Landsea, Isaac Held, James P. Kossin, A. K. Srivastava and Masato Sugi. 2010. "Tropical
25 cyclones and climate change." *Nature Geoscience* 3(3):157-163.
- 26 Knutson, T. R., Sirutis, J. J., Vecchi, G. A., Garner, S., Zhao, M., Kim, H.-S., et al. (2013).
27 Dynamical Downscaling Projections of Twenty-First-Century Atlantic Hurricane Activity:
28 CMIP3 and CMIP5 Model-Based Scenarios. *Dx.Doi.org*. doi:10.1175/JCLI-D-12-00539.1
- 29 Korty, Robert L., Suzana J. Camargo and Joseph Galewsky. 2012a. "Tropical Cyclone
30 Genesis Factors in Simulations of the Last Glacial Maximum." *Journal of Climate* 25(12).
- 31 Korty, Robert L., Suzana J. Camargo and Joseph Galewsky. 2012b. "Variations in Tropical
32 Cyclone Genesis Factors in Simulations of the Holocene Epoch." *Journal of Climate* 25(23).
- 33 Kossin, James P., Kerry A. Emanuel and Gabriel A. Vecchi. 2014. "The poleward migration
34 of the location of tropical cyclone maximum intensity." *Nature* 509(7500):349-352.
- 35 Koutavas, Athanasios, Jean Lynch-Stieglitz, Thomas M. Marchitto and Julian P. Sachs. 2002.
36 "El Nino-like pattern in ice age tropical Pacific sea surface temperature." *Science*
37 297(5579):226-230.
- 38 Kuhnert, Henning, Holger Kuhlmann, Mahyar Mohtadi, Helge Meggers, Karl-Heinz
39 Baumann and Jürgen Pätzold. 2014. "Holocene tropical Western Indian Ocean sea surface
40 temperatures in covariation with climatic changes in the Indonesian region."
41 *Paleoceanography*.
- 42 Lewis, Simon and Maslin, Mark (2014). "Defining the Anthropocene." *Nature*, 519, 171–180
43 doi:10.1038/nature14258.

- 1 Li, Lijuan, Pengfei Lin, Yongqiang Yu, Bin Wang, Tianjun Zhou, Li Liu, Jiping Liu, Qing
2 Bao, Shiming Xu, Wenyu Huang, Kun Xia, Ye Pu, Li Dong, Si Shen, Yimin Liu, Ning Hu,
3 Mimi Liu, Wenqi Sun, Xiangjun Shi, Weipeng Zheng, Bo Wu, Mirong Song, Hailong Liu,
4 Xuehong Zhang, Guoxiong Wu, Wei Xue, Xiaomeng Huang, Guangwen Yang, Zhenya Song
5 and Fangli Qiao. 2013. "The flexible global ocean-atmosphere-land system model, Grid-point
6 Version 2: FGOALS-g2." *Advances in Atmospheric Sciences* 30(3):543-560.
- 7 Luan, Y., P. Braconnot, Y. Yu, W. Zheng and O. Marti. 2012. "Early and mid-Holocene
8 climate in the tropical Pacific: seasonal cycle and interannual variability induced by insolation
9 changes." *Clim. Past Discuss.* 8(1):505-555.
- 10 Lucas, Christopher, Bertrand Timbal and Hanh Nguyen. 2014. "The expanding tropics: a
11 critical assessment of the observational and modeling studies." *Wiley Interdisciplinary
12 Reviews: Climate Change* 5(1):89-112.
- 13 Menkes, Christophe E., Matthieu Lengaigne, Patrick Marchesiello, Nicolas C. Jourdain,
14 Emmanuel M. Vincent, Jérôme Lefèvre, Fabrice Chauvin and Jean-Francois Royer. 2012.
15 "Comparison of tropical cyclogenesis indices on seasonal to interannual timescales." *Climate
16 dynamics* 38(1-2):301-321.
- 17 Merlis, T. M., Zhao, M., & Held, I. M. (2013). The sensitivity of hurricane frequency to ITCZ
18 changes and radiatively forced warming in aquaplanet simulations. *Geophysical Research
19 Letters*, 40(15), 4109–4114. doi:10.1002/grl.50680
- 20 Montgomery, Michael T., Roger K. Smith and Sang V. Nguyen. 2010. "Sensitivity of
21 tropical-cyclone models to the surface drag coefficient." *Quarterly Journal of the Royal
22 Meteorological Society* 136(653):1945-1953.
- 23 Nolan, David S. and Eric D. Rappin. 2008. "Increased sensitivity of tropical cyclogenesis to
24 wind shear in higher SST environments." *Geophysical Research Letters* 35(14):L14805.
- 25 O'Brien, C., Foster, G., Martínez-Botí, M., Abell, R., Rae, J. and Pancost, R., 2014. High sea
26 surface temperatures in tropical warm pools during the Pliocene. *Nature Geoscience*, 7(8),
27 pp.606-611.
- 28 Pagani, M., Liu, Z., LaRiviere, J., and Ravelo, A.C., 2009. "High Earth-system climate
29 sensitivity determined from Pliocene carbon dioxide concentrations." *Nature Geoscience*
30 3(1):27-30.
- 31 Ravelo, A. C., Lawrence, K. T., Fedorov, A., and Ford, H. L., 2014. Comment on "A 12-
32 million-year temperature history of the tropical Pacific Ocean". *Science*, 346(6216), 1467-
33 1467.
- 34 Riemer, M., M. T. Montgomery and M. E. Nicholls. 2013. "Further examination of the
35 thermodynamic modification of the inflow layer of tropical cyclones by vertical wind shear."
36 *Atmos. Chem. Phys.* 13(1):327-346.
- 37 Rimbu, N., G. Lohmann, S. J. Lorenz, J. H. Kim and R. R. Schneider. 2004. "Holocene
38 climate variability as derived from alkenone sea surface temperature and coupled ocean-
39 atmosphere model experiments." *Climate Dynamics* 23(2):215-227.
- 40 Robinson, Marci M., Harry J. Dowsett and Mark A. Chandler. 2008. "Pliocene role in
41 assessing future climate impacts." *Eos, Transactions American Geophysical Union*
42 89(49):501-502.

- 1 Saint-Lu, M., Braconnot, P., Leloup, J., Lengaigne, M., & Marti, O. (2015). Changes in the
2 ENSO/SPCZ relationship from past to future climates. *Earth and Planetary Science Letters*,
3 412, 18–24. <http://doi.org/10.1016/j.epsl.2014.12.033>
- 4 Stott, Lowell, Kevin Cannariato, Robert Thunell, Gerald H. Haug, Athanasios Koutavas and
5 Steve Lund. 2004. "Decline of surface temperature and salinity in the western tropical Pacific
6 Ocean in the Holocene epoch." *Nature* 431(7004):56-59.
- 7 Sueyoshi, T., R. Ohgaito, A. Yamamoto, M. O. Chikamoto, T. Hajima, H. Okajima, M.
8 Yoshimori, M. Abe, R. O'Ishi, F. Saito, S. Watanabe, M. Kawamiya and A. Abe-Ouchi. 2013.
9 "Set-up of the PMIP3 paleoclimate experiments conducted using an Earth system model,
10 MIROC-ESM." *Geosci. Model Dev.* 6(3):819-836.
- 11 Tippett, Michael K., Suzana J. Camargo and Adam H. Sobel. 2010. "A Poisson Regression
12 Index for Tropical Cyclone Genesis and the Role of Large-Scale Vorticity in Genesis."
13 *Journal of Climate* 24(9):2335-2357.
- 14 Tory, K. J., R. A. Dare, N. E. Davidson, J. L. McBride and S. S. Chand. 2012. "The
15 importance of low-deformation vorticity in tropical cyclone formation."
- 16 Vecchi, G. A., Swanson, K. L., & Soden, B. J. (2008). Whither hurricane activity. *Science*,
17 322(5902), 687. doi:10.1126/science.1164396
- 18 Velden, Christopher S. and John Sears. 2014. "Computing Deep-Tropospheric Vertical Wind
19 Shear Analyses for Tropical Cyclone Applications: Does the Methodology Matter?" *Weather*
20 *and Forecasting*.
- 21 Villarini, G., and Vecchi, G. 2012: North Atlantic Power Dissipation Index (PDI) and
22 Accumulated Cyclone Energy (ACE): Statistical Modeling and Sensitivity to Sea Surface
23 Temperature Changes. *J. Climate*, **25**, 625–637. doi:10.1175/JCLI-D-11-00146.1
- 24 Waelbroeck, C., et al. (2009). Constraints on the magnitude and patterns of ocean cooling at
25 the Last Glacial Maximum. *Nature Geoscience*, 2(2), 127–132. doi:10.1038/ngeo411
- 26 Webster, Peter J., Greg J. Holland, Judith A. Curry and H. R. Chang. 2005. Changes in
27 tropical cyclone number, duration, and intensity in a warming environment. *Science*,
28 309(5742), 1844-1846.
- 29 Zhang, Y. G., Pagani, M., & Liu, Z., 2014a. A 12-million-year temperature history of the
30 tropical Pacific Ocean. *Science*, 344(6179), 84-87.
- 31 Zhang, Y., Pagani, M. and Liu, Z., 2014b. Response to Comment on "A 12-million-year
32 temperature history of the tropical Pacific Ocean". *Science*, 346(6216), pp.1467-1467.
- 33

1 **Tables**

2 Table 1. Trace gases and Earth's orbital parameters recommended for PMIP. The precession
 3 is specified with respect to NH autumnal equinox.

| Period | CO ₂ (ppmv) | CH ₄ (ppbv) | N ₂ O (ppbv) | Eccentricity | Obliquity (°) | Angular Precession (°) |
|------------------------------------|---------------------------|---------------------------|----------------------------|--------------|------------------|---------------------------|
| Pliocene (3Ma) | 405 | 760 | 270 | 0.016724 | 23.446 | 102.04 |
| LGM (21ka) | 185 | 350 | 200 | 0.018994 | 22.949 | 114.42 |
| mid-Holocene (6ka) | 280 | 650 | 270 | 0.018682 | 24.105 | 0.87 |
| Preindustrial (Control) | 280 | 760 | 270 | 0.016724 | 23.446 | 102.04 |

4

5 Table 2. List of GCMs used in this study. The *b* factor in the right column is incorporated in
 6 the GPI such that preindustrial control TC genesis frequencies are calibrated to 90 annual
 7 occurrences for each GCM. HadGEM2-ES and MIROC4m are only used for the single time
 8 periods as indicated. The preindustrial simulation in PlioMIP for HadCM3 shows different
 9 behaviour that that of the PMIP simulations and so requires a different normalisation factor, *b*.

| Model | Atmospheric Resolution °Lat x °Lon x Levels | <i>b</i> (x10 ⁻⁵) | Standard Deviation (%) | Reference |
|------------------------------------|---|----------------------------------|------------------------------|----------------------|
| CCSM4 | 0.9 × 1.25 × 26 | 6.2 | 1.7 | Gent et al. 2011 |
| FGOALS-G2 | 2.8 × 2.8 × 26 | 2.7 | 1.1 | Li et al. 2013 |
| HADCM3 (PlioMIP value) | 2.5 × 3.75 × 19 | 5.8 (1.5) | 2.9 | Gordon et al. 2000 |
| HADGEM2-ES (RCP8.5 only) | 1.25 × 1.875 × 38 | 2.7 | - | Collins et al. 2011 |
| IPSL-CM5A | 3.75 × 1.875 × 39 | 2.4 | 1.6 | Dufresne et al. 2013 |
| MIROC-ESM | 2.8 × 2.8 × 80 | 1.6 | 2.5 | Sueyoshi et al. 2013 |
| MIROC4m (Pliocene only) | 2.8 × 2.8 × 20 | 0.8 | - | Chan et al. 2011 |

10

1 7 Figures

2

3 Figure 1. Sea surface temperature (contour lines) and potential intensity in northern
4 hemisphere (NH) during Jul-Oct (JASO) and southern hemisphere (SH) during Jan-Apr
5 (JFMA) for (a) preindustrial control, (b) Pliocene, (c) LGM and (d) mid-Holocene. Units are
6 SST ($^{\circ}\text{C}$) and potential intensity (ms^{-1}).

7

8 Figure 2. Preindustrial control GPI from (a) CCSM4, (b) FGOALS-G2, (c) HadCM3, (d)
9 IPSL-CM5A-LR, (e) MIROC-ESM and (f) the Ensemble Mean. Northern hemisphere depicts
10 JASO monthly mean GPI while southern hemisphere depicts JFMA monthly mean GPI. Units
11 are 10^{-13} normalised occurrences $\text{m}^{-2} \text{month}^{-1}$

12

13 Figure 3. The difference in genesis potential index between mid-Holocene and PI in northern
14 hemisphere (JASO) and southern hemisphere (JFMA) for (a) CCSM4, (b) FGOALS, (c)
15 HadCM3, (d) IPSL, (e) MIROC. Units are 10^{-13} normalised occurrences $\text{m}^{-2} \text{month}^{-1}$

16 Figure 4. (a) mid-Holocene ensemble GPI (b) mid-Holocene and preindustrial control
17 ensemble GPI difference, and (c) Robustness of the palaeoclimate genesis signals, as
18 indicated by the number of models agreeing with the direction of the change. Yellow and red
19 denote areas for model agreement on positive sign change. Green and blue areas denote model
20 agreement on negative sign change. Northern hemisphere depicts JASO season, while
21 southern hemisphere depicts JFMA season. Units in (a) and (b) are 10^{-13} normalised
22 occurrences $\text{m}^{-2} \text{month}^{-1}$.

23

24 Figure 5. The difference in genesis potential index between LGM and preindustrial in
25 northern hemisphere (JASO) and southern hemisphere (JFMA) for (a) CCSM4, (b) FGOALS,
26 (c) HadCM3, (d) IPSL, (e) MIROC. Units are 10^{-13} normalised occurrences $\text{m}^{-2} \text{month}^{-1}$

27

28 Figure 6. (a) LGM ensemble GPI (b) LGM and preindustrial control ensemble GPI difference,
29 and (c) Robustness of the ensemble signals, as indicated by the number of models agreeing
30 with the direction of the change. Yellow and red denote areas for model agreement on
31 positive sign change. Green and blue areas denote model agreement on negative sign change.
32 White areas denote regions where less than four models agree. Northern hemisphere depicts
33 JASO season, while southern hemisphere depicts JFMA season. Units in (a) and (b) are 10^{-13}
34 normalised occurrences $\text{m}^{-2} \text{month}^{-1}$

35

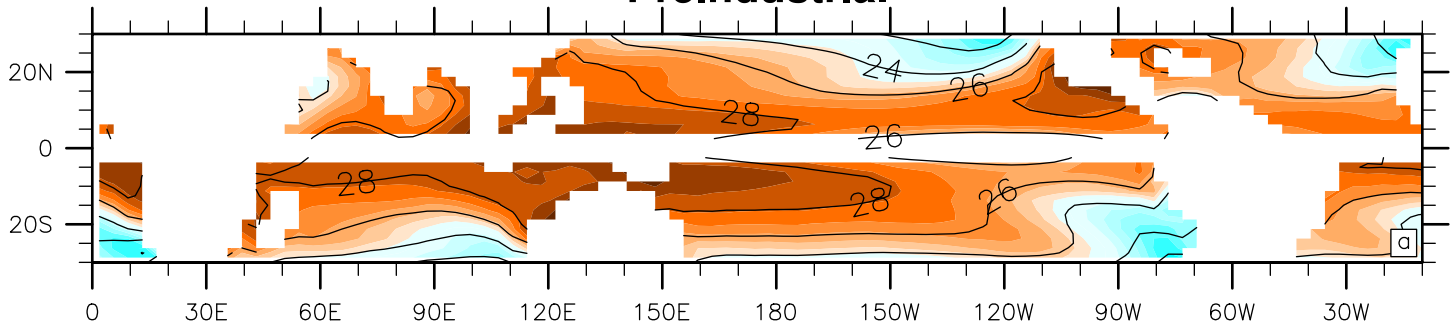
36 Figure 7. Change in genesis potential index between Pliocene and preindustrial in northern
37 hemisphere (JASO) and southern hemisphere (JFMA) for (a) CCSM4, (b) FGOALS, (c)
38 HadCM3, (d) IPSL, (e) MIROC. Units are in 10^{-13} normalised occurrences $\text{m}^{-2} \text{month}^{-1}$

39

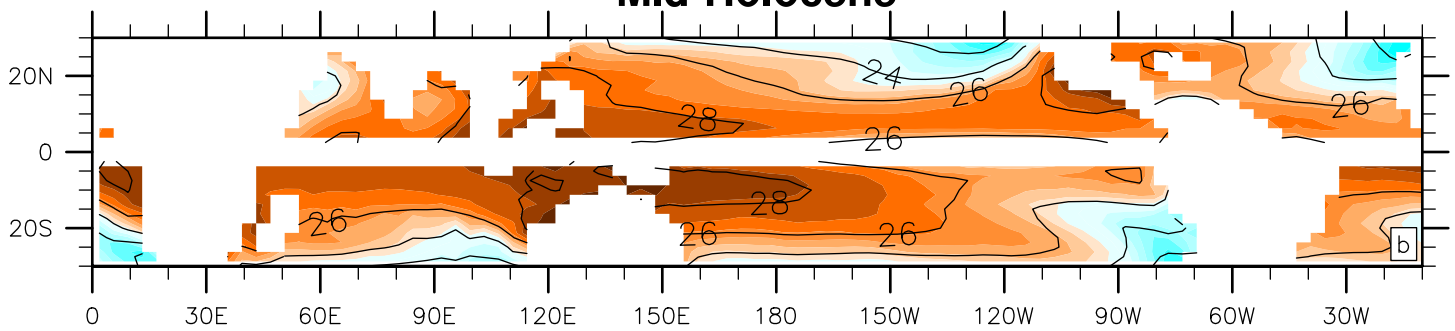
40 Figure 8. (a) Pliocene ensemble GPI (b) Pliocene and preindustrial control ensemble GPI
41 difference, and (c) Robustness of the ensemble signals, as indicated by the number of models
42 agreeing with the direction of the change. Yellow and red denote areas for model agreement
43 on positive sign change. Green and blue areas denote model agreement on negative sign
44 change. White areas denote regions where less than four models agree. Northern hemisphere
45 depicts JASO season while southern hemisphere depicts JFMA season. Units in (a) and (b)
46 are 10^{-13} normalised occurrences $\text{m}^{-2} \text{month}^{-1}$

- 1
- 2 Figure 9. Model and ensemble mean cumulative annual, global genesis potential index as
- 3 percentage of preindustrial control value.
- 4
- 5 Figure 10. Ensemble monthly cumulative genesis potential intensity for the different time
- 6 periods over (a) the northern hemisphere and (b) the southern hemisphere.
- 7
- 8 Figure 11. RCP8.5 annual cyclone genesis frequency projection between 2005-2095. The
- 9 shaded area represents the spread expected from internal variability alone, from the baseline
- 10 of 90 cumulative occurrences observed in modern day (black dashed line).

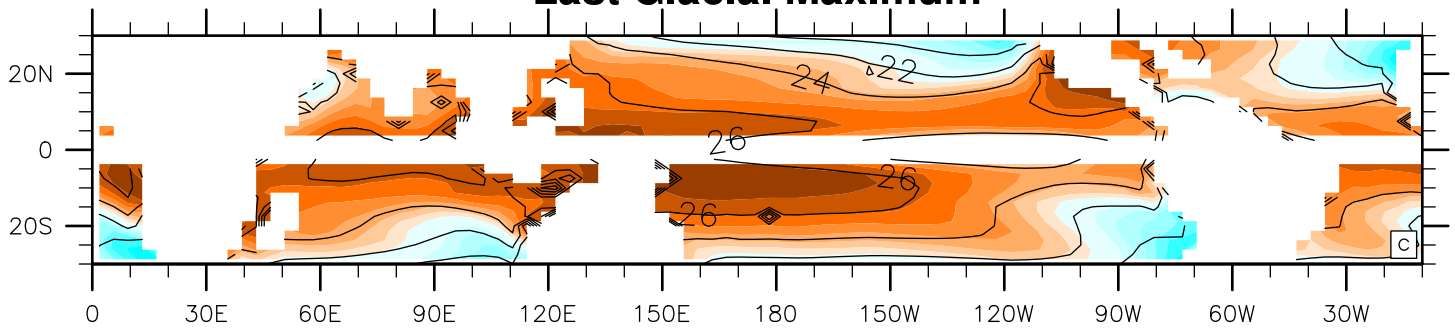
Preindustrial



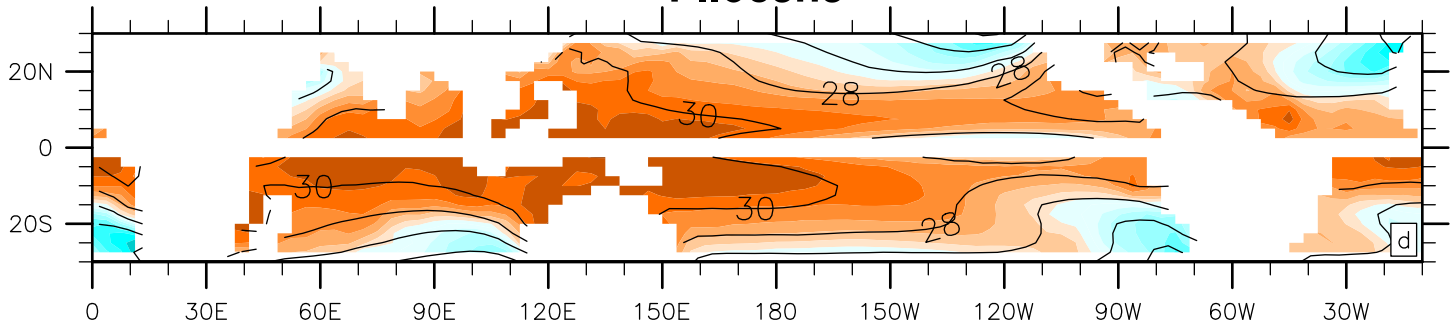
Mid-Holocene



Last Glacial Maximum

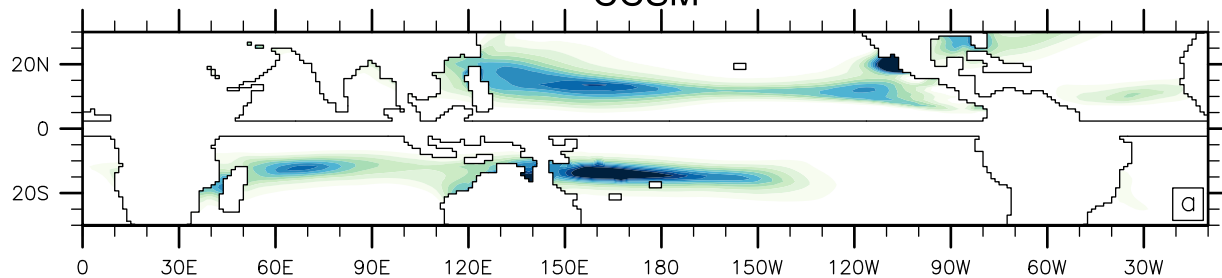


Pliocene

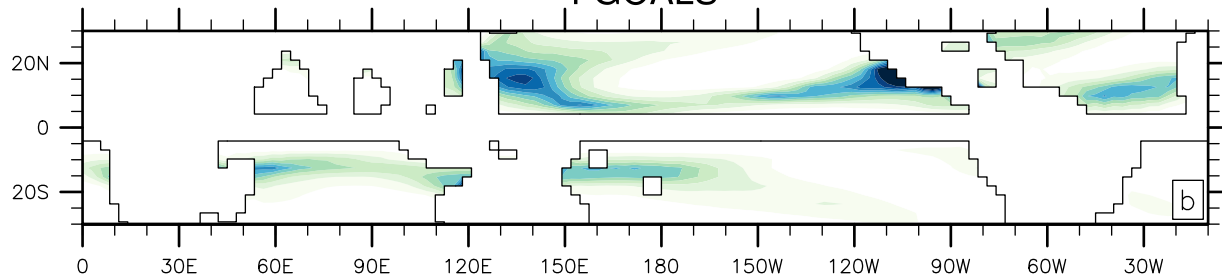


Potential Intensity (m/s)

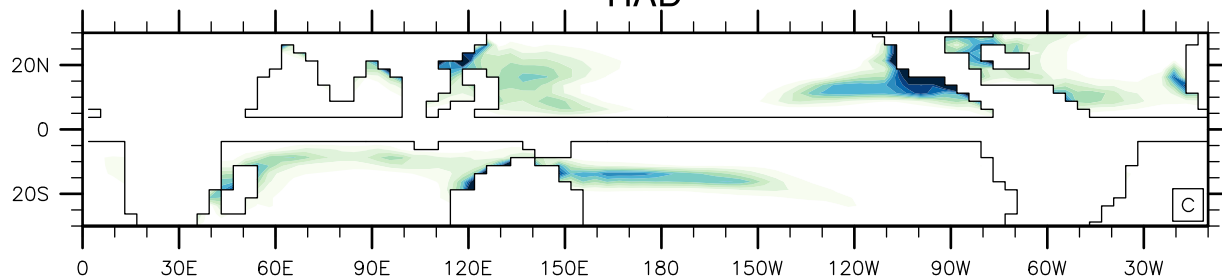
CCSM



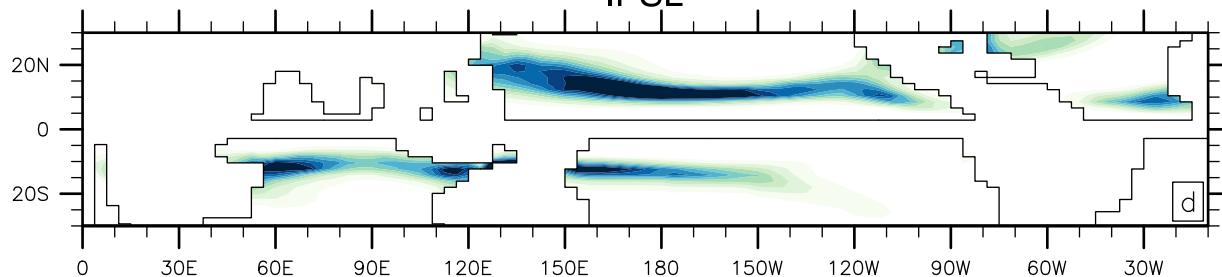
FGOALS



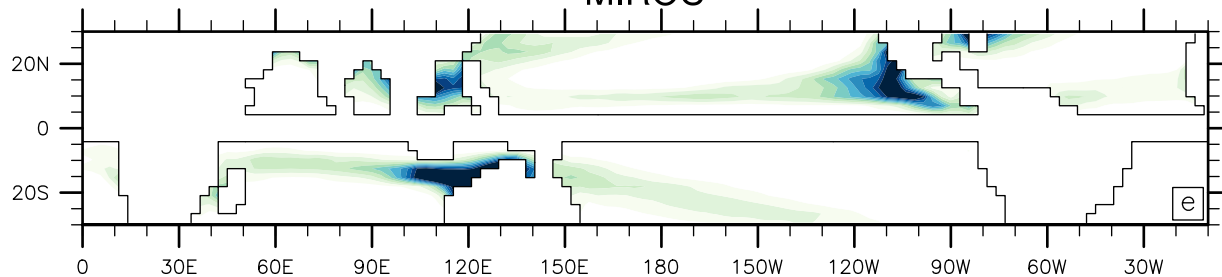
HAD



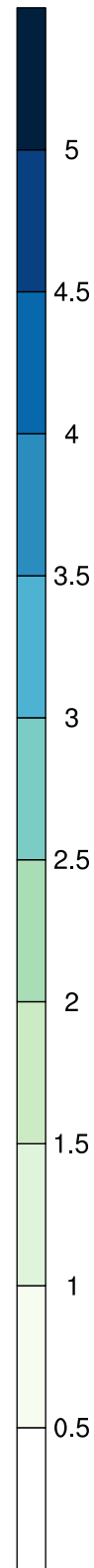
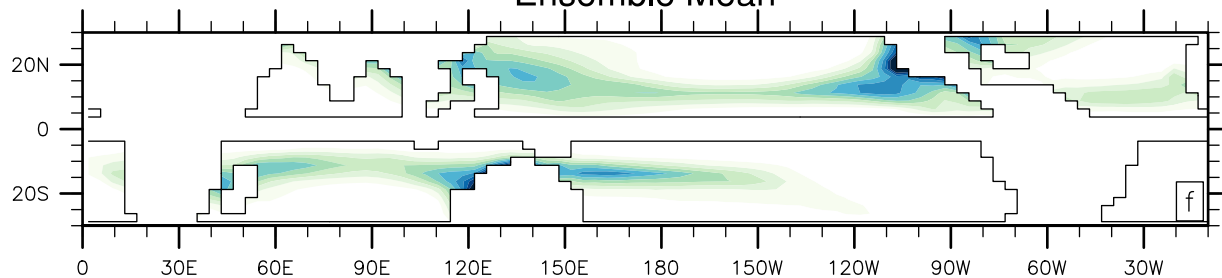
IPSL



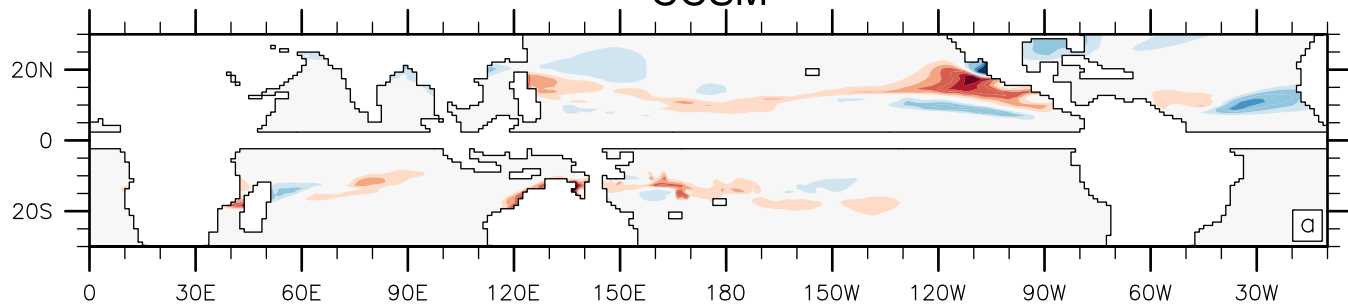
MIROC



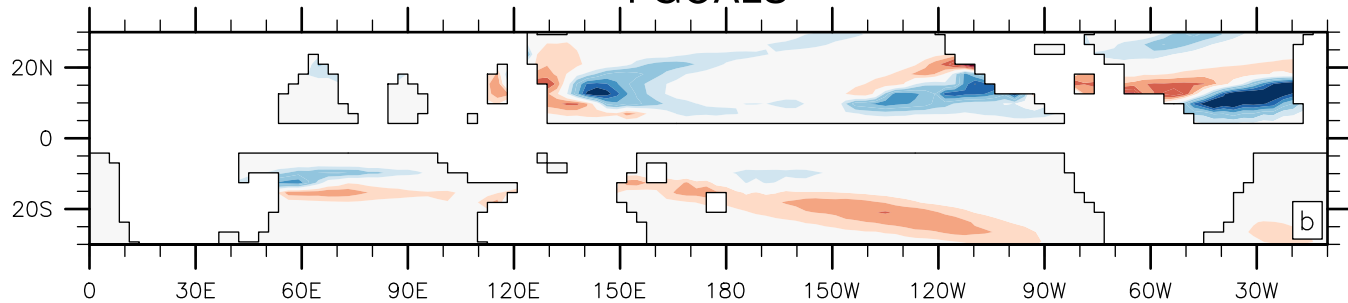
Ensemble Mean



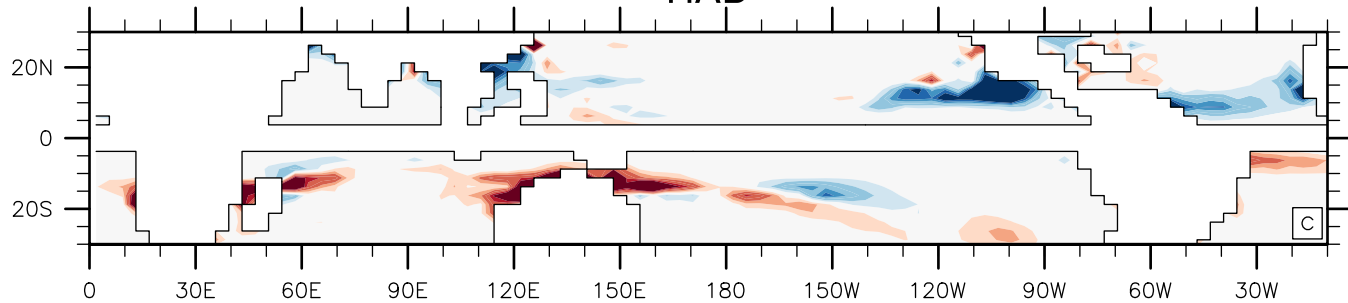
CCSM



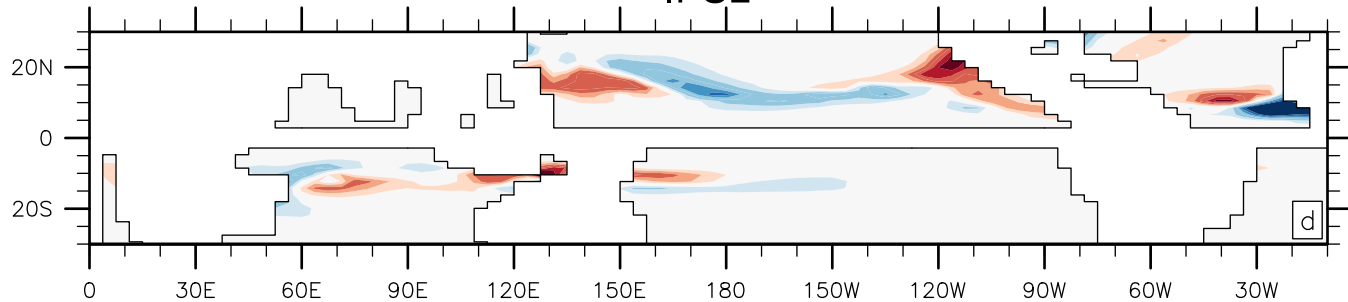
FGOALS



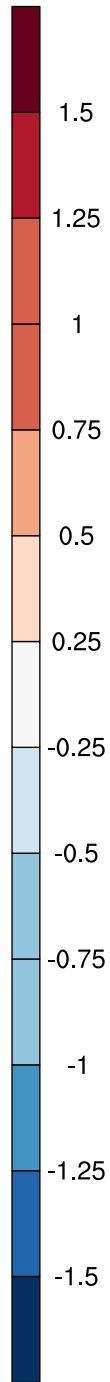
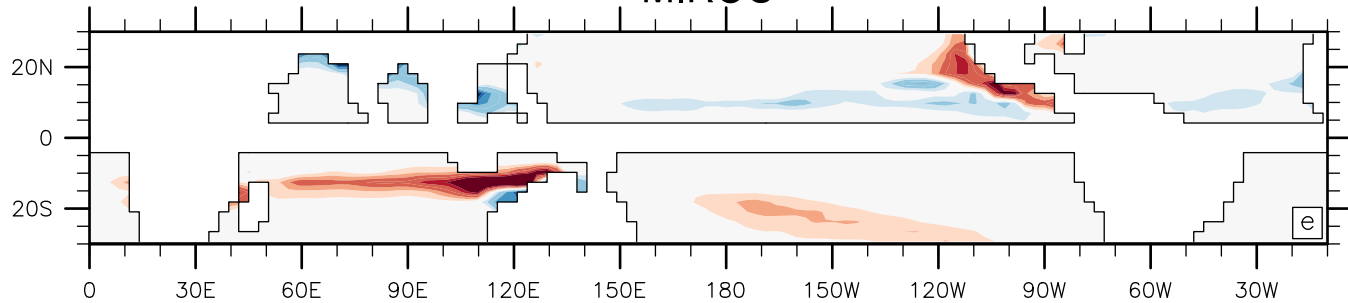
HAD



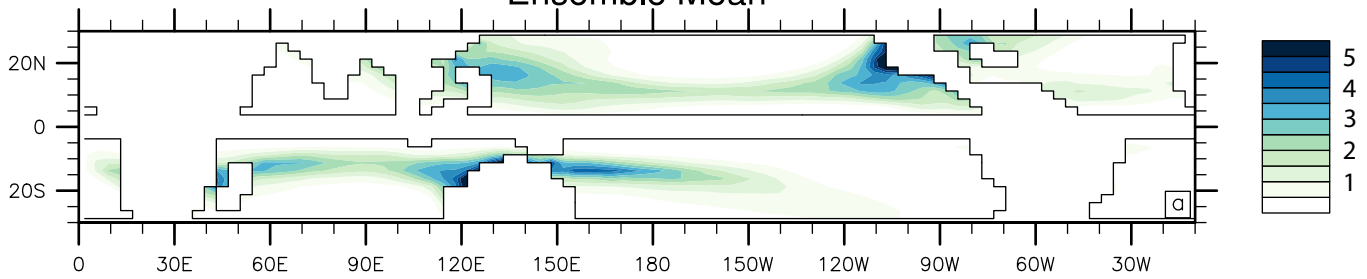
IPSL



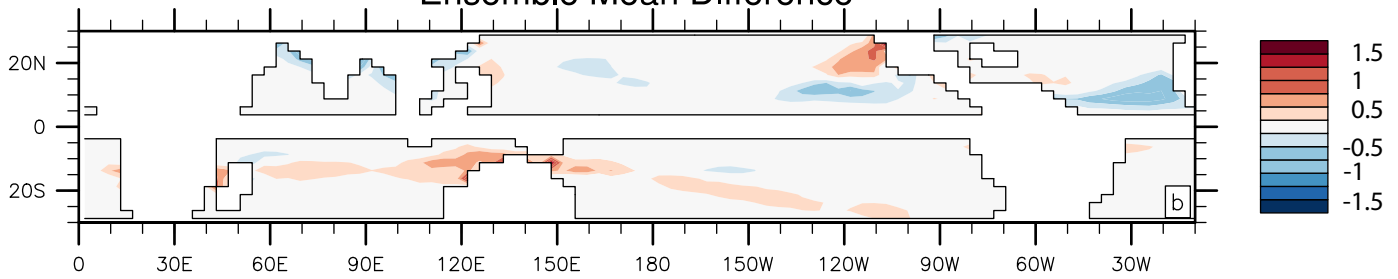
MIROC



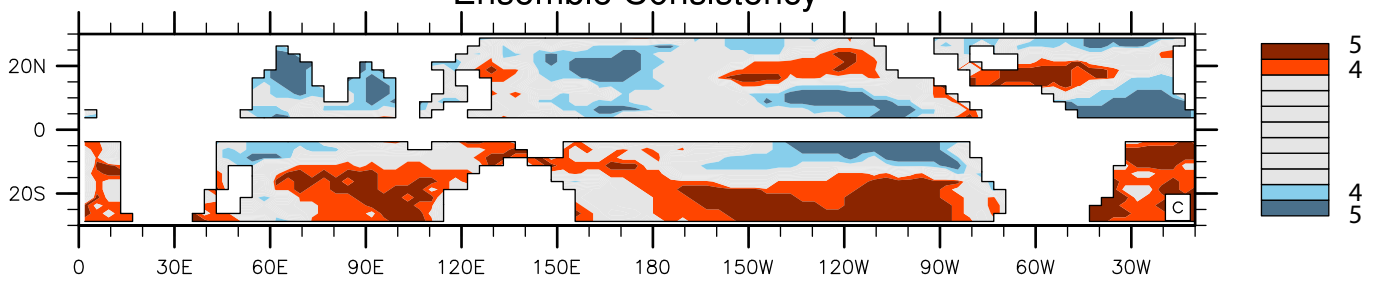
Ensemble Mean



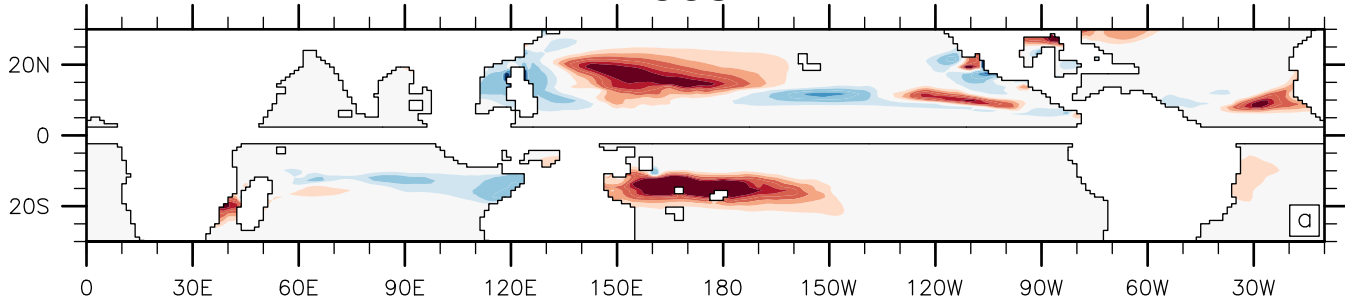
Ensemble Mean Difference



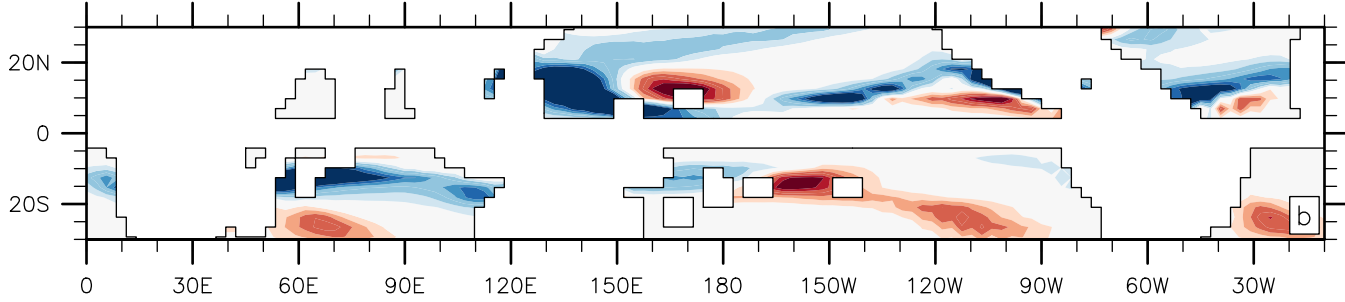
Ensemble Consistency



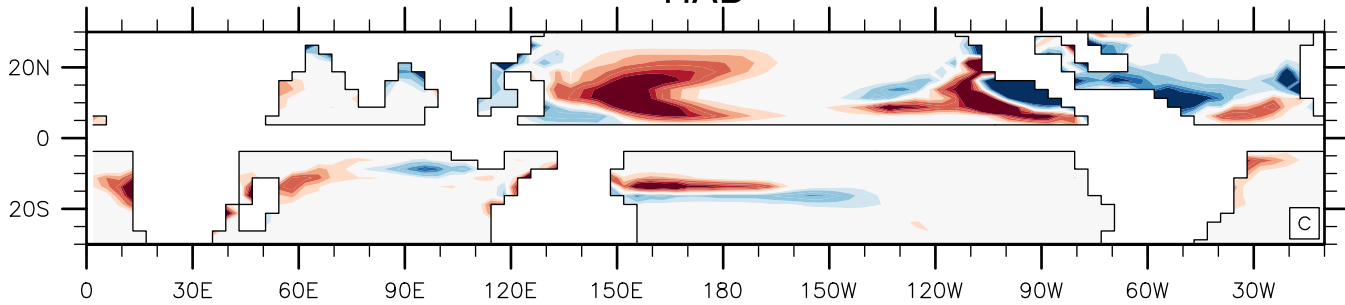
CCSM



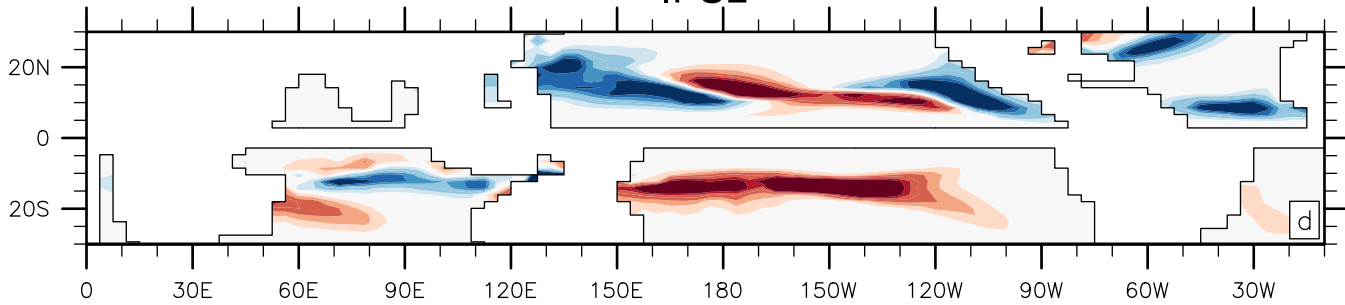
FGOALS



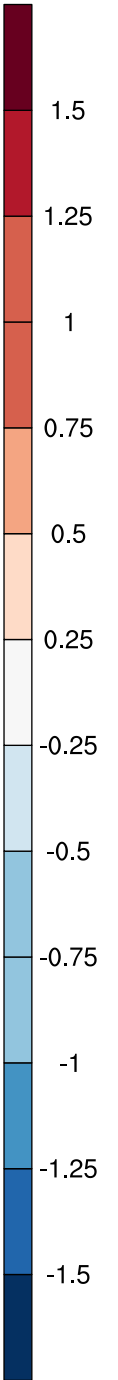
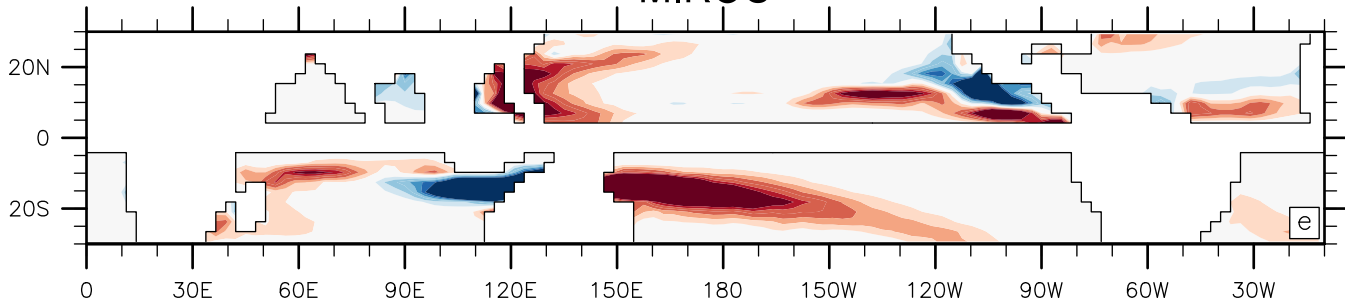
HAD



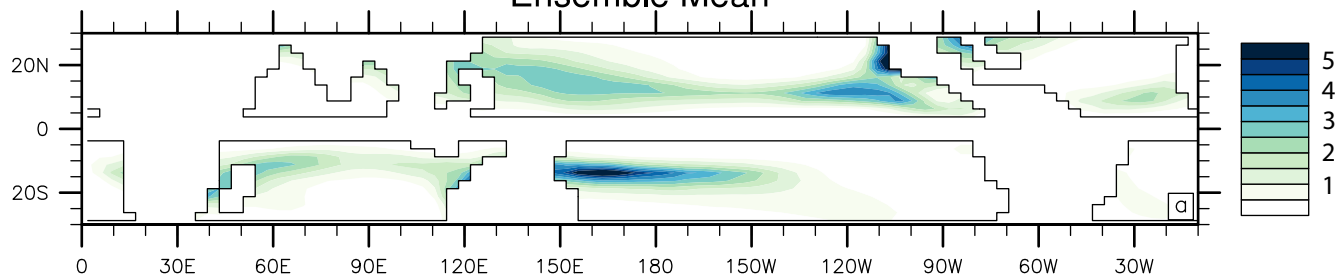
IPSL



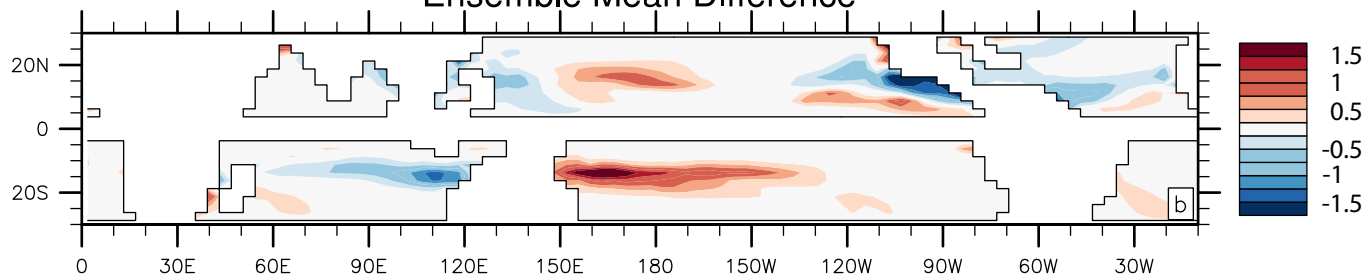
MIROC



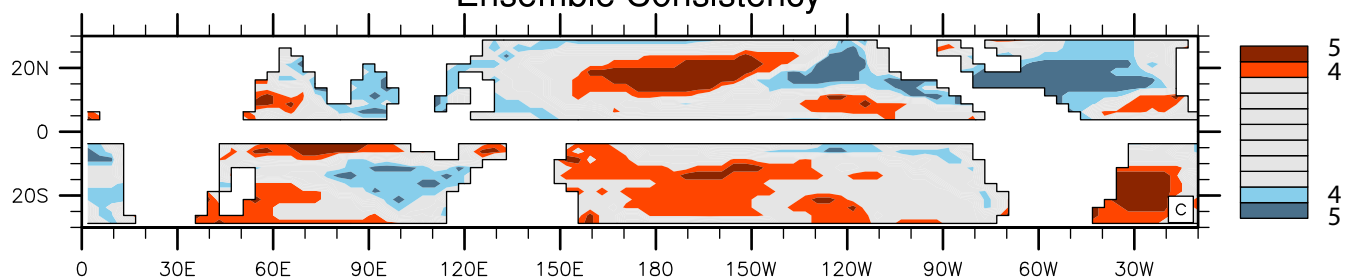
Ensemble Mean



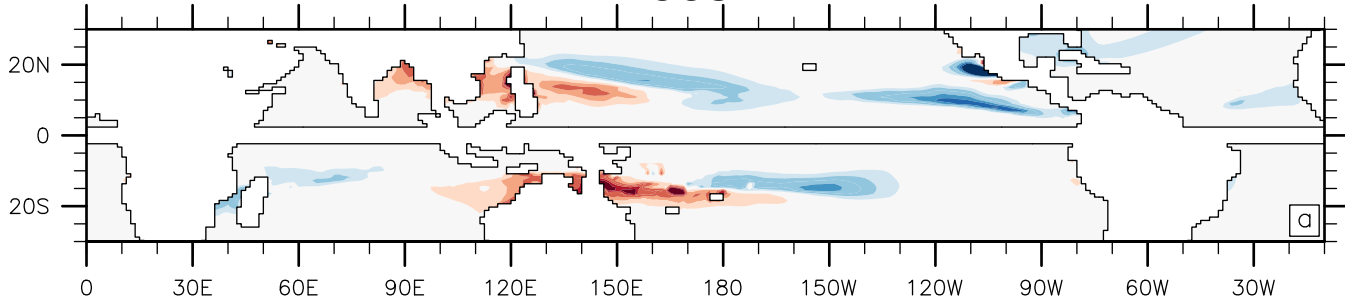
Ensemble Mean Difference



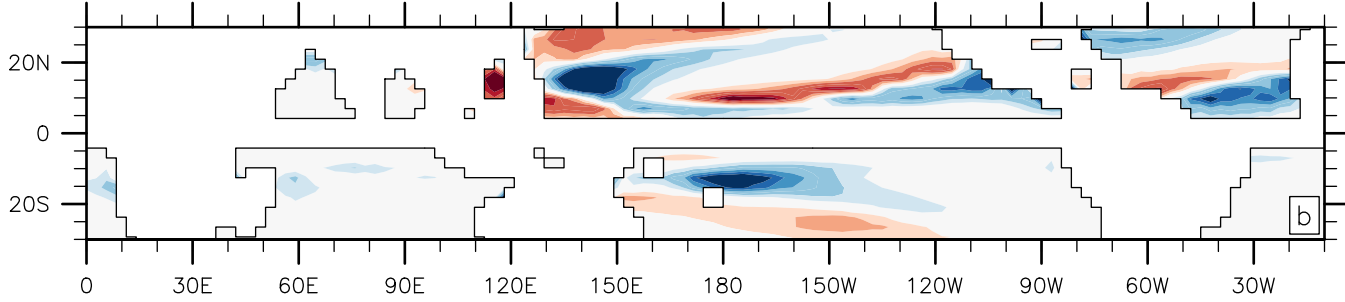
Ensemble Consistency



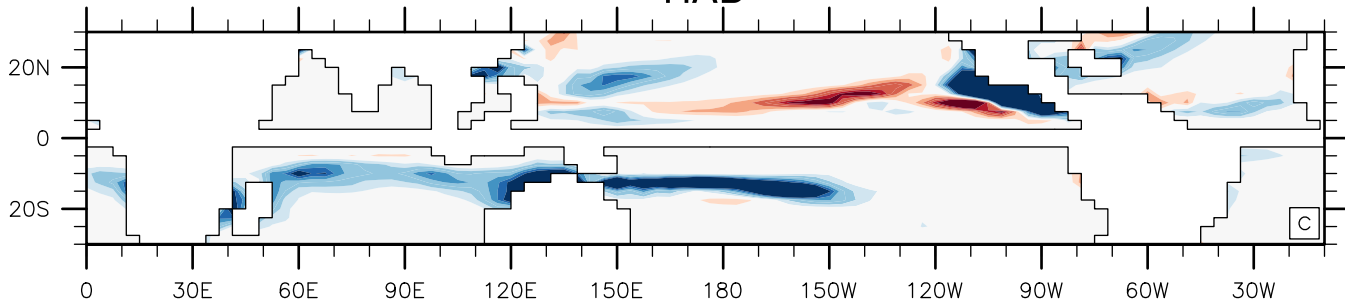
CCSM



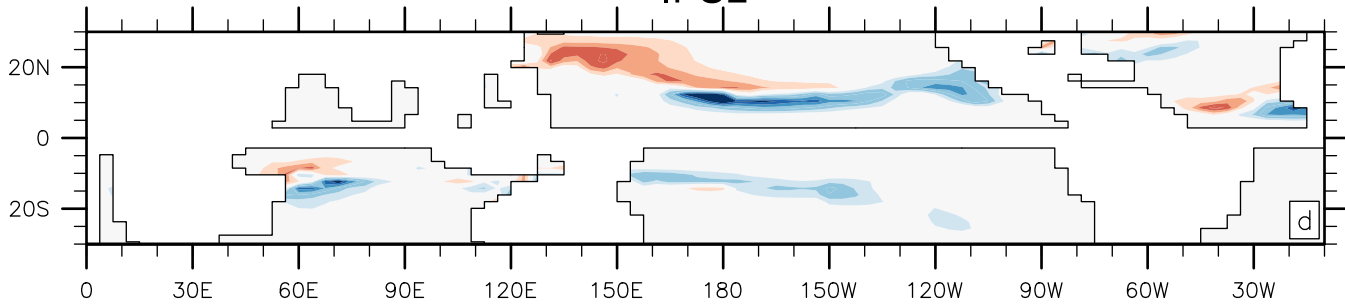
FGOALS



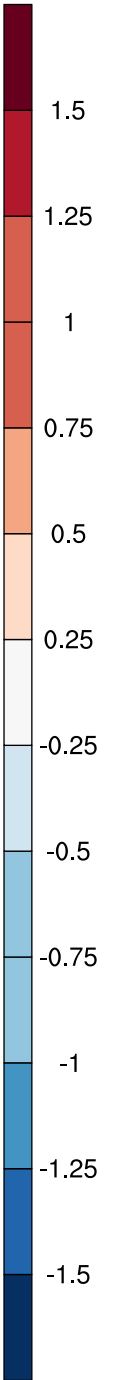
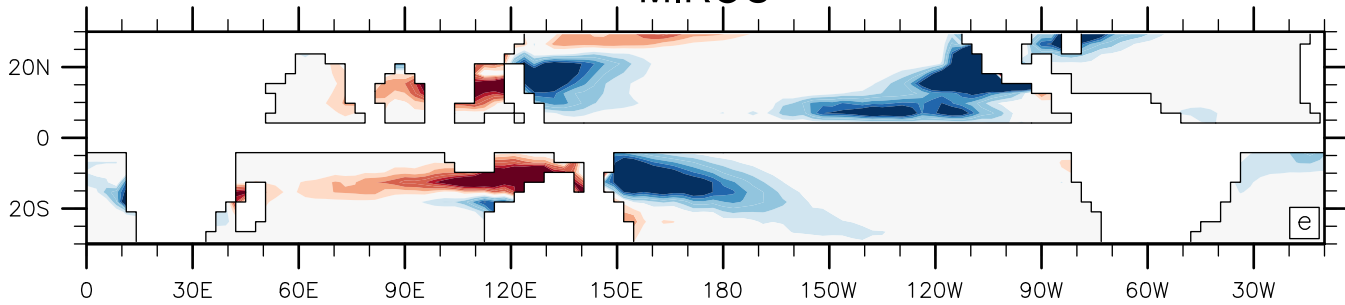
HAD



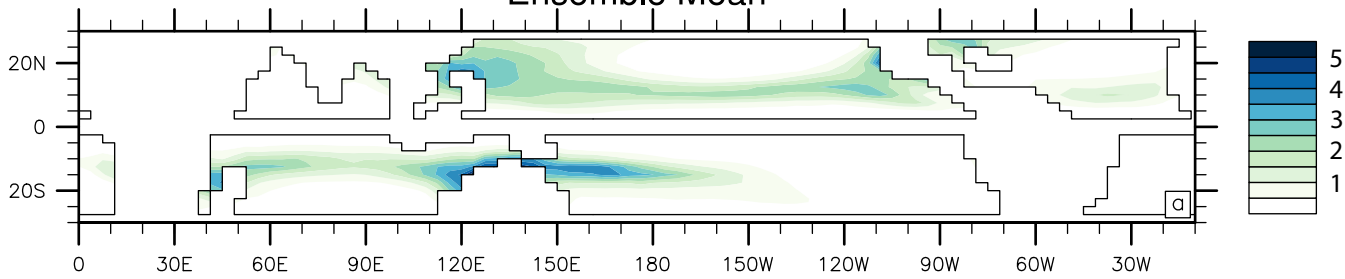
IPSL



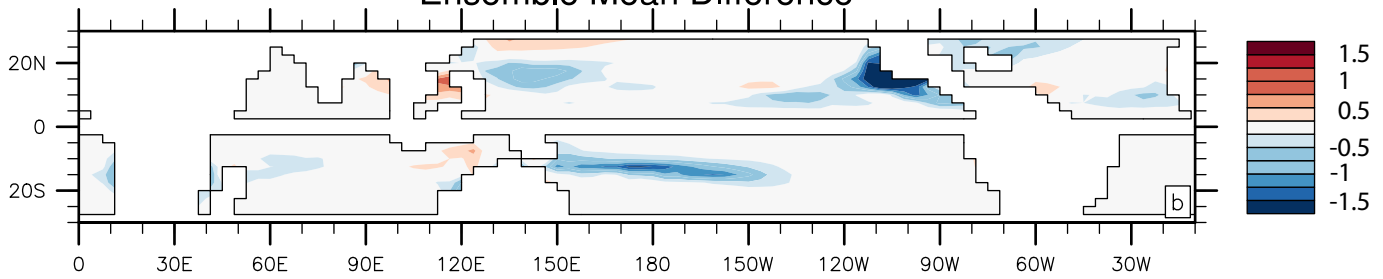
MIROC



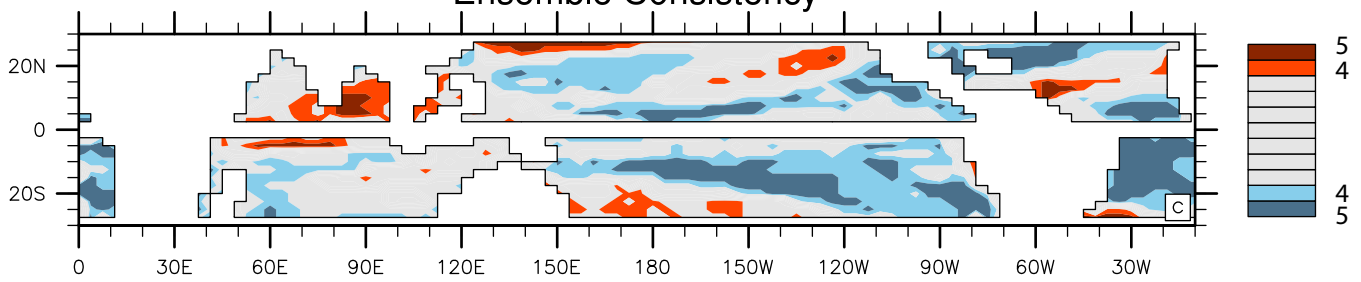
Ensemble Mean

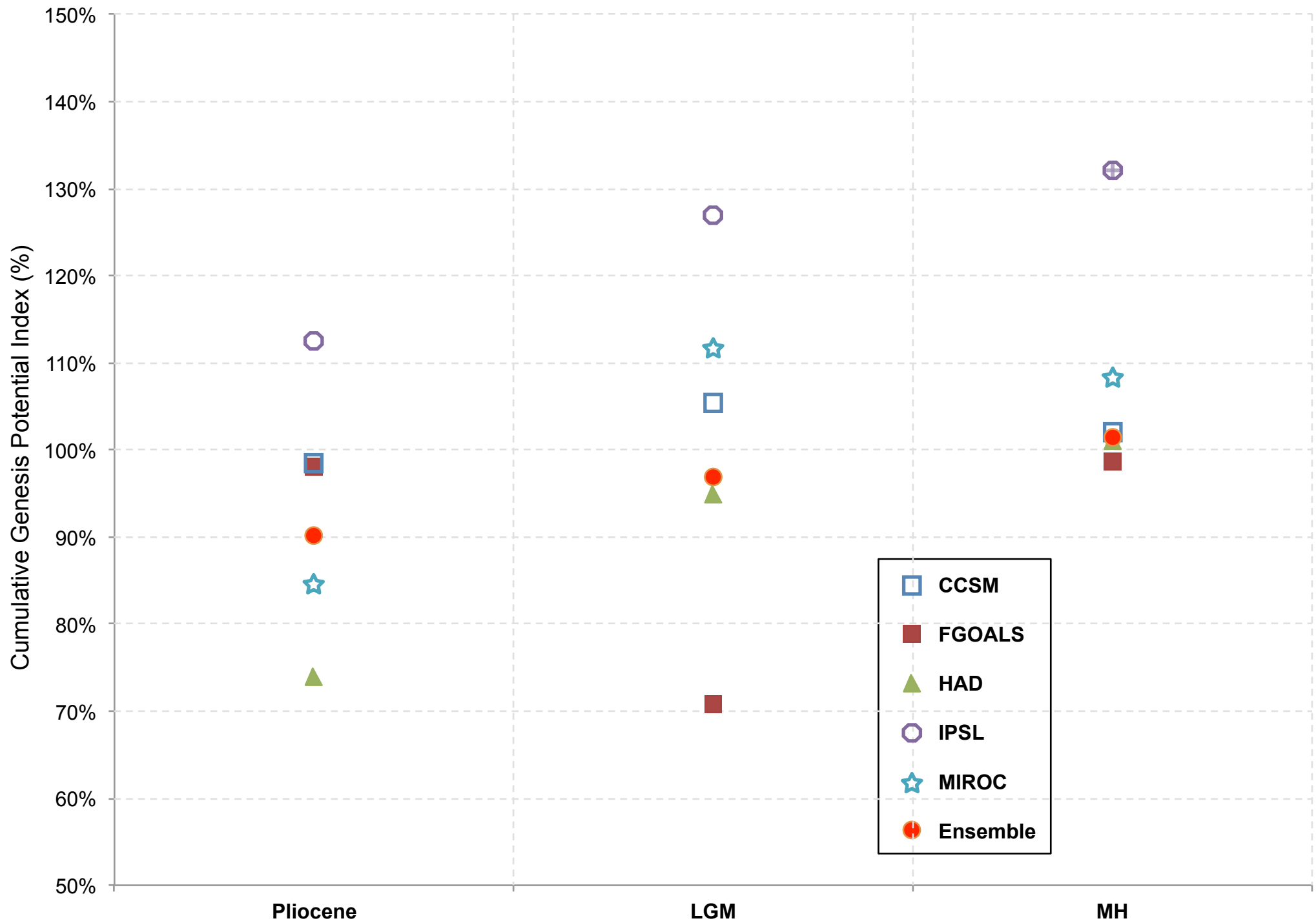


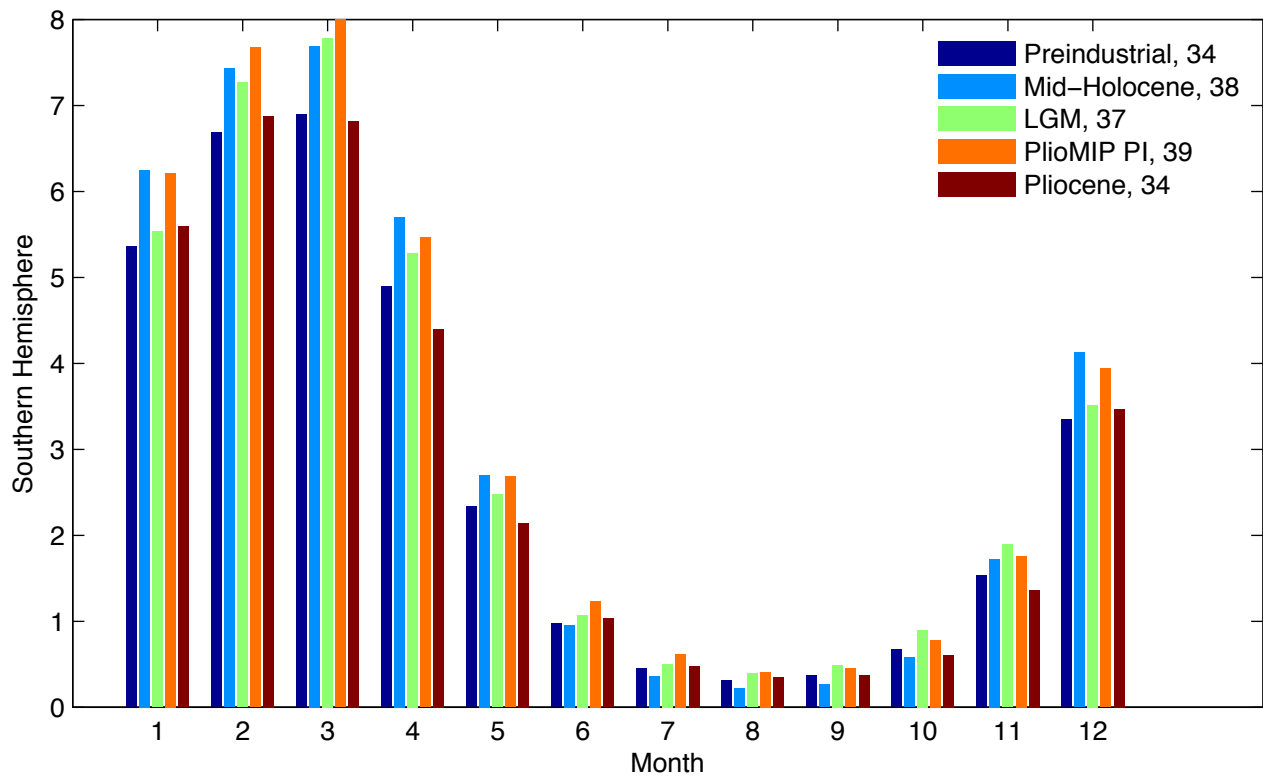
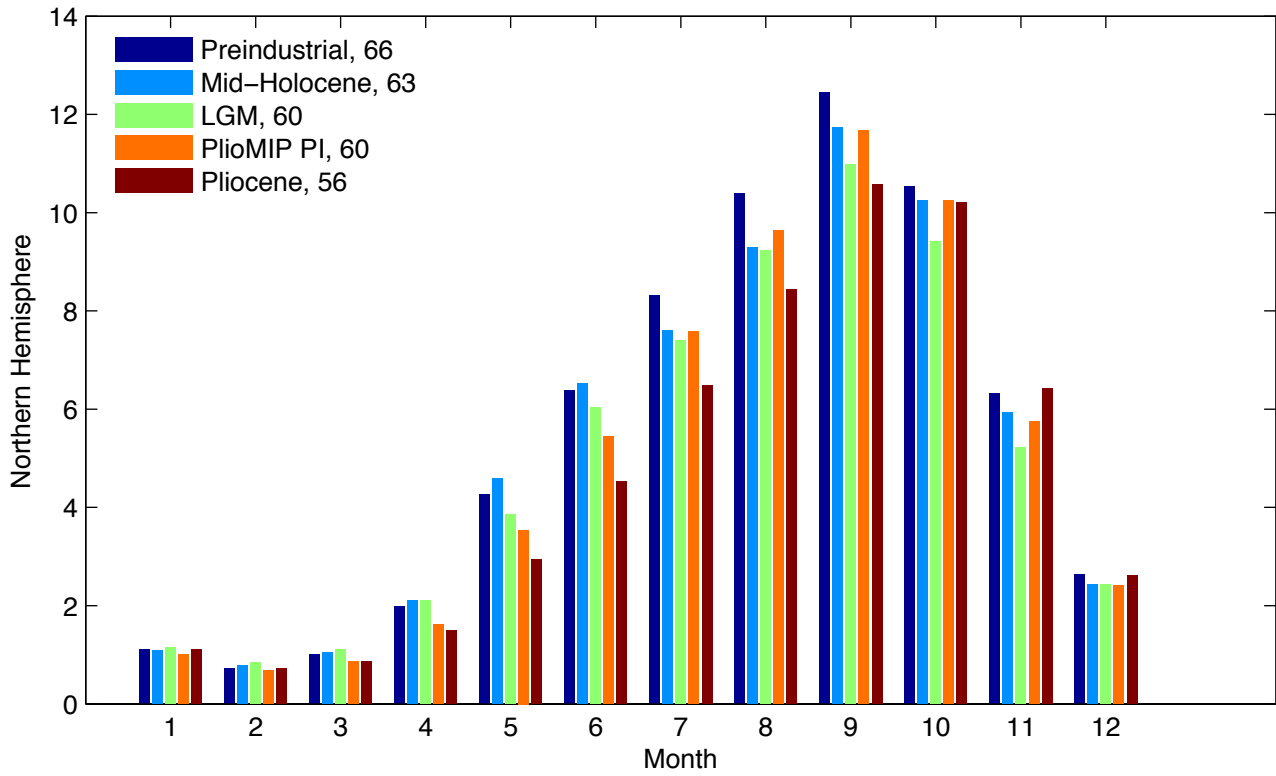
Ensemble Mean Difference



Ensemble Consistency







RCP 8.5

